Extreme precipitation, exacerbated by anthropogenic climate change, drove Peru's record-breaking 2023 dengue outbreak

Mallory J. Harris[1,2,*], Jared T. Trok[3], Kevin S. Martel[4,5], Mercy J. Borbor Cordova[6,7], Noah S. Diffenbaugh[3,8], César V. Munayco[4], Andrés G. Lescano[5], and Erin A. Mordecai[1]

[1]Department of Biology, Stanford University, USA
[2]Department of Biology, University of Maryland, USA
[3]Department of Earth System Science, Stanford University, Stanford, USA
[4]Centro Nacional de Epidemiología, Prevención y Control de Enfermedades, Peru
[5]School of Public Health and Administration, Universidad Peruana Cayetano Heredia, Peru
[6]Pacific International Center for Disaster Risk Reduction (PIC-RRD), Escuela Superior Politecnica del Litoral (ESPOL), Ecuador
[7]Faculty of Maritime Engineering and Sea Sciences, Escuela Superior Politecnica del Litoral (ESPOL), Ecuador
[8]Doerr School of Sustainability, Stanford University, Stanford, USA
[*]corresponding author (mharr15@umd.edu)

Contents

1 Introduction **3**

2 Methods **6**
2.1 Climate, case, and vulnerability index data 6
2.2 Identifying cyclone-affected districts 7
2.3 Matching 7
2.4 Generalized synthetic control 8
2.5 Examining associations between climate, vulnerability indices and cyclone-attributable incidence 9
2.6 Quantifying the influence of historical climate forcing on the probability of extreme March precipitation in northwestern Peru 10

3 Results **11**
3.1 Districts with the most anomalous precipitation during Cyclone Yaku generally had warm, dry climates 11
3.2 Cyclone Yaku caused 67% of dengue cases in the cyclone-affected districts 12
3.3 Cyclone-attributable incidence varied with housing quality, hydrology, and temperature 13
3.4 Extreme precipitation in March in northwestern Peru is 42% more likely due to historical climate forcing 17

4 Discussion **18**

5 Works Cited **23**

6 Supplemental Materials **37**
6.1 Main methods and results 38
6.1.1 Debiasing temperature data 38
6.1.2 Comparing imbalance between cyclone-affected and control districts before and after matching 42
6.2 Sensitivity analyses 52
6.2.1 Sensitivity to exclusion of climate covariates in model . . 52
6.2.2 Sensitivity to exclusion of non-coastal districts from control pool 53
6.2.3 Sensitivity to use of temperature-dependent R_0 as climate covariate in model 56
6.2.4 Sensitivity to including observations prior to 2016 57
6.2.5 Sensitivity to excluding observations from 2020 - 2021 . . 58
6.2.6 Sensitivity to upper and lower precipitation anomaly thresholds 59
6.2.7 Sensitivity to number of matched units 62
6.2.8 Sensitivity to number of latent factors 63
6.2.9 Analysis at the region level 63

Abstract Anthropogenic forcing is increasing the likelihood and severity of certain extreme weather events, which may catalyze outbreaks of climate-sensitive infectious diseases. Extreme precipitation events can promote the spread of mosquito-borne illnesses by creating vector habitat, destroying infrastructure, and impeding vector control. Here, we focus on Cyclone Yaku, which caused heavy rainfall in northwestern Peru from March 7th - 20th, 2023 and was followed by the worst dengue outbreak in Peru's history. We apply generalized synthetic control methods to account for baseline climate variation and unobserved confounders when estimating the causal effect of Cyclone Yaku on dengue cases across the 56 districts with the greatest precipitation anomalies. We estimate that 67 (95% CI: 30 - 87) % of cases in cyclone-affected districts were attributable to Cyclone Yaku. The cyclone significantly increased cases for over six months, causing 38,209 (95% CI: 17,454 - 49,928) out of 57,246 cases. The largest increases in dengue incidence due to Cyclone Yaku occurred in districts with a large share of low-quality roofs and walls in residences, greater flood risk, and warmer temperatures above $24°C$. Analyzing an ensemble of climate model simulations, we found that extremely intense March precipitation in northwestern Peru is 42% more likely in the current era compared to a preindustrial baseline due to climate forcing. In sum, extreme precipitation like that associated with Cyclone Yaku has become more likely with climate change, and Cyclone Yaku caused the majority of dengue cases across the cyclone-affected districts.

Significance Statement

Anthropogenic climate change is increasing the risk of extreme events that can lead to infectious disease epidemics, but few studies have directly measured this health cost of climate change. We do so by focusing on Cyclone Yaku, which affected northwestern Peru in March 2023, and was immediately followed by a dengue epidemic. Cyclone Yaku caused 67% of cases reported over six months in the affected region. Industrial-era climate forcing has increased the likelihood of extreme March precipitation like that associated with Cyclone Yaku by 42%. Assessing the linkages between climate change, extreme weather, and outbreaks of dengue and other infectious diseases is crucial for understanding the impact that climate change has already had and preparing for future health risks.

1 Introduction

Human activities are driving major changes to the climate system, including more frequent and intense extreme weather events such as heat waves, droughts, and cyclones (Seneviratne et al. 2021; National Academies of Sciences, Engineering, and Medicine 2016). Climate change may increase risk of an array of adverse health outcomes including heat-related deaths, Lyme disease, and foodborne illness connected to the bacteria *Vibrio vulnificus* (Vezzulli et al. 2016). (National

Academies of Sciences, Engineering, and Medicine 2016; Ebi et al. 2020; Hegerl et al. 2010; Vicedo-Cabrera et al. 2021; Chapman et al. 2022; Ogden et al. 2014; McPherson et al. 2017; Vezzulli et al. 2016). Mosquito-borne diseases may be particularly sensitive to climate change because several transmission-relevant biological rates (e.g., biting rate and development time) vary with temperature, while aquatic vector breeding habitat is associated with precipitation (Mordecai et al. 2019, 2017; Shocket et al. 2020).

Assessing linkages between anthropogenic climate change and health outcomes may guide adaptation efforts while ensuring that the social and environmental costs of fossil fuel emissions are weighed accurately in litigation and climate policy (Stuart-Smith et al. 2021; Burger et al. 2020; Limaye et al. 2020; Ebi et al. 2020; Scovronick et al. 2019). However, very few studies have attempted to quantify the contribution of historical climate change to mosquito-borne disease burden (e.g., (Carlson et al. 2023; Childs et al. 2024)), and these studies focused on the contribution of long-term increases in mean temperature to vector-borne disease burden. As a result, a critical gap remains with respect to the contribution of anthropogenic climate change-driven extreme weather to vector-borne disease outbreaks, though extreme weather has been shown to trigger and exacerbate infectious disease outbreaks (Alcayna et al. 2022; Mora et al. 2022; Carlson et al. 2024).

Reported cases of dengue, a virus transmitted by *Aedes aegypti* and *Aedes albopictus*, have surged to unprecedented levels in recent years, with a total of over five million cases and 5,000 associated deaths reported globally in 2023, and over ten million cases reported in 2024 with large epidemics across the Americas (World Health ORganization 2023; Pan American Health Organization / World Health Organization 2024). There has been some speculation that extreme weather (particularly heavy rainfall and flooding) is a primary driver of this expansion in transmission (World Health ORganization 2023), given that dengue outbreaks are strongly associated with favorable temperature and precipitation conditions (Caldwell et al. 2021; Nova et al. 2021; Lowe et al. 2018). Previous studies found that heavy rainfall and tropical cyclone exposure were associated with increased risk of dengue, but these studies applied non-causal methods, which may not accurately capture the contribution of a specific event to a given outbreak (Li et al. 2022; Lowe et al. 2018; Adeola et al. 2017). Isolating the effects of particular weather phenomena requires accounting for multiple time-varying drivers that influence dengue transmission (e.g., strain introductions, immunity, mobility, vector control, and urbanization), which are often inadequately captured by existing data sources and modeling approaches (Zhang et al. 2020; Nova et al. 2021; Giesen et al. 2020; Ogden 2017). A generalized synthetic control approach can overcome these methodological challenges by accounting for time trends that may vary across space with unobserved covariates to isolate the effects of an exposure (i.e., extreme weather event) across impacted areas (Xu 2017). Generalized synthetic controls and related quasi-experimental methods have previously been applied in diverse epidemiological and environmental contexts (Bruhn et al. 2017; Shioda et al. 2021; Nyathi et al. 2019; Sheridan et al. 2022; Schwarz et al. 2023), but these methods have not yet been applied

to assess how extreme weather events contribute to infectious disease outbreaks.

Here, we use generalized synthetic control methods to quantify the causal contribution of extreme precipitation to an unprecedented dengue outbreak in Peru. In March of 2023, Peru experienced anomalously heavy precipitation due to a coastal El Niño and Cyclone Yaku, a severe cyclone that primarily affected northwestern coastal Peru (Peng et al. 2024; Munayco et al. 2024; Bagcchi 2023). The cyclone had extensive impacts, with 460,000 people affected by flooding, approximately 40,000 people left without homes, and 83 people reported dead (United Nations Office for the Coordination of Humanitarian Affairs 2023). Shortly after, Peru experienced the worst dengue outbreak in the country's history. By the end of July 2023, cases exceeded the five-year average by a factor of ten and 381 dengue-related deaths had been reported (Munayco et al. 2024). It has been postulated that this outbreak was linked to anomalous precipitation, but the causal contribution of Cyclone Yaku to dengue cases in Peru has not been examined, limiting estimates of the true scope of damage caused by this particular extreme weather event.

Additional climate and socioeconomic factors may moderate the effects of extreme weather on dengue incidence. For example, built environment (e.g., water infrastructure and housing quality) and human behavior (e.g., water storage practices) may mediate the relationship between extreme weather and dengue transmission (Gibb et al. 2023; Mulligan et al. 2015; Alcayna et al. 2022; Reiter et al. 2003). Housing built from low-quality materials and informal settlements may both facilitate contact between humans and mosquitoes and increase vulnerability to damage from extreme weather (Mulligan et al. 2015; Borbor-Cordova et al. 2020). The relationship between extreme precipitation and dengue risk is also nonlinear and context-dependent: flooding may promote vector breeding habitat, but can reduce transmission by flushing out vector habitat (Caldwell et al. 2021). Dry settings with limited water access may promote transmission as people store water near their residences (Lowe et al. 2018; Stewart Ibarra et al. 2013; Lowe et al. 2021). Temperature may also moderate the effects of extreme precipitation on outbreak potential, given known temperature-sensitivity of mosquitoes and evidence that large epidemics of mosquito-borne disease may only occur within a range of suitable temperatures ($25 - 29°C$) (Mordecai et al. 2017; Caldwell et al. 2021; Skaff et al. 2020). Identifying factors associated with greater risk of large dengue outbreaks following extreme weather events may help guide vector control and public health emergency preparedness (Udayanga et al. 2020).

Finally, quantifying the extent to which historical anthropogenic climate forcing has influenced the likelihood of extreme precipitation in northwest Peru is an important step toward tracing potential linkages between climate change and human health. In general, extreme weather events are becoming more frequent and intense as anthropogenic climate change accelerates (Seneviratne et al. 2021; National Academies of Sciences, Engineering, and Medicine 2016). Attribution studies have quantified the contribution of anthropogenic forcing to particular extreme weather conditions, including heat waves, heavy rainfall, hurricanes, and droughts (Trok et al. 2024; Diffenbaugh et al. 2015; Van Old-

enborgh et al. 2017; Diffenbaugh et al. 2017; Emanuel 2017). Although most places are likely to experience increases in precipitation intensity at higher levels of climate forcing, the influence of historical climate change on the likelihood of extreme precipitation events varies between regions, underscoring the importance of tailoring attribution analyses to particular geographic areas (Chand et al. 2022; Reed et al. 2022; Murakami et al. 2017; Seneviratne et al. 2021; Diffenbaugh et al. 2017). Climate model simulations suggest that both human activity and coastal El Niño conditions increased the likelihood of extreme precipitation across the entire country of Peru in March 2017 (Christidis et al. 2019), but no such analysis has focused on observed conditions in the region of northwestern Peru associated with Cyclone Yaku.

This study contributes to both our understanding of the drivers and impacts of Cyclone Yaku and the relationships between anthropogenic forcing, extreme weather, and human health more broadly. First, we construct a generalized synthetic control model to estimate how many additional dengue cases were caused by Cyclone Yaku across the cyclone-affected districts in Peru. Next, we examine associations between cyclone-attributable dengue burden and district-level characteristics to identify factors that may moderate dengue risk following extreme precipitation. Finally, we conduct a climate attribution analysis to test whether anthropogenic forcing has increased the risk of extreme precipitation events like Cyclone Yaku in northwestern Peru. These analyses may inform context-specific public health and risk reduction measures for dengue and other weather-sensitive diseases.

2 Methods

We used a quasi-experimental generalized synthetic control approach to estimate the number of cyclone-attributable cases by comparing observed cases in cyclone-affected districts to a hypothetical counterfactual estimate of cases without the cyclone. Our model accounted for weather conditions and latent trends estimated from a control group of cyclone-unaffected districts with similar baseline climate. Analyses were conducted in R version 4.2.1 (R Core Team 2022). The Stanford University Institutional Review Board determined that this project does not involve human subjects. Code to conduct analyses are available on Github at https://github.com/mjharris95/yaku-dengue.

2.1 Climate, case, and vulnerability index data

Mean temperature and total precipitation reported hourly in the ECMWF ERA5-Land Hourly reanalysis dataset were extracted at the district level using Google Earth Engine (Copernicus Climate Change Service (C3S) 2017). Given evidence of negative bias in this dataset compared to weather stations, particularly at high elevations, we debiased hourly temperature following Childs et al. (2024) (see subsubsection 6.1.1). We then calculated the daily average temperature and total precipitation across each district by taking a population-

weighted average (e.g., weighting by the proportion of the total population living in a given 100m x 100m grid cell, estimated for 2020 by WorldPop (Edwards et al. 2021)).

Weekly case reports (probable and confirmed) by district (administrative division 3) in Peru from 2010 - 2023 were provided by CDC Peru. The main analysis spanned 2016 through 2023, and a sensitivity analysis included all observations from 2010 onward (subsubsection 6.2.4). We additionally conducted an analysis at the region level (administrative division 1) with matching to regions in other countries (subsubsection 6.2.9). Incidence was calculated by dividing reported cases by population size, estimated annually by the Oficina General de Tecnologías del Ministerio de Salud (OGTI, General Office of Information Technology of the Ministry of Health) based on census data. Vulnerability indices for cyclone-affected districts were accessed through CDC Peru, which compiled data from other sources (Table 5).

2.2 Identifying cyclone-affected districts

We constrained our analysis to the 561 districts that reported cases of dengue in 2023. Cyclone Yaku, which was first detected by El Servicio Nacional de Meteorología e Hidrología del Perú (the National Service of Meteorology and Hydrology of Peru, SENAMHI) on March 7th, 2023 and dissipated on March 20th, primarily impacted the northernwestern coast of Peru (from Tumbes in the north to La Libertad in the south, Figure 1A) (SENAMHI 2023).

Given that there was no map of districts most affected by Cyclone Yaku, we defined cyclone-affected districts as those that received anomalously high precipitation between March 7 - 20, 2023. Anomalies were defined as the difference between mean daily precipitation across this time period in 2023 compared to the historic reference years 1993 - 2022 excluding 2017, another year with extreme El Niño conditions. We plotted the distribution of precipitation anomalies across all districts to identify a cutoff value to distinguish cyclone-affected districts from cyclone-unaffected control districts. Specifically, districts with anomalies exceeding 8 mm/day were cyclone-affected and districts with anomalies below 7.5 mm/day were cyclone-unaffected.

2.3 Matching

There are several distinct climatic zones within Peru (from west to east: the dry Pacific coastline, the cool Andes mountains, and the warm and wet Amazon rainforest (Figure 1B,C), which may exhibit substantially different dengue dynamics (Chowell et al. 2011). If the control pool includes cyclone-unaffected districts with baseline climate conditions that are substantially different from those of the cyclone-affected districts, the generalized synthetic control model may overfit to latent trends that are not relevant to the cyclone-affected area. We therefore used matching to further filter down the set of cyclone-unaffected districts to a control pool with recent temperature and precipitation trends most similar to the cyclone-affected districts. We aggregated daily temperature and

precipitation to four-week averages to smooth over short-term variation and conducted matching across the 67 observations from the beginning of 2018 until Cyclone Yaku. Using the PanelMatch package we identified the ten cyclone-unaffected districts most similar climatically to each cyclone-affected district based on Mahalanobis distance, a metric that favors units where the relationship between temperature and precipitation is similar to that in the cyclone-affected districts (Imai et al. 2023; Kim et al. 2022; R Core Team 2022; Mahalanobis 1936). We tested whether the analysis was affected by the number of control districts to which each cyclone-affected district was matched or including all cyclone-unaffected districts in the control pool without matching (Figure 23).

Cyclone-unaffected districts that were matched to at least one cyclone-affected district were included in the control pool used to construct the generalized synthetic control (Figure 8), effectively filtering out cyclone-unaffected districts with climate conditions least similar to those across the cyclone-affected districts. In a sensitivity analysis, we examined the effects of limiting the potential control pool to districts in coastal regions (Figure 16). To evaluate alignment between the cyclone-affected districts and the matched control districts, we calculated standardized difference as the difference between each cyclone-affected district and its matched control districts at a given time point divided by the standard deviation of the corresponding climate variable across all observations.

2.4 Generalized synthetic control

We estimated the effect of Cyclone Yaku on dengue cases in the cyclone-affected districts using a generalized synthetic control model (Xu 2017).

The dengue incidence (Y) in a given spatial unit (i) at each four-week time period (t) was estimated as:

$$Y_{i,t} = \delta_{i,t} D_{i,t} + \dot{x}_{i,t}^{\intercal} \dot{\beta} + \dot{\lambda}_i^{\intercal} \dot{f}_t + e_{it}$$

where δ is the effect of the cyclone and D is a dummy variable indicating cyclone-affected districts following the cyclone; $\dot{x}$ is a vector of climate covariates (precipitation and temperature) with coefficients $\dot{\beta}$; $\dot{f}$ and $\dot{\lambda}$ are latent factors and factor loadings, respectively, comprise interactive fixed effects (explained in further detail below); and e is an error term.

We used interactive fixed effects to control for unobserved time-varying confounders like strain-specific immunity, vector control, and human movement, which may have different trends and influence across space. A set of n *latent factors* are defined where each latent factor is a time series of constants across the study period. In turn, each spatial unit is assigned a *factor loading*, or vector that weights each latent factor. In other words, the interactive fixed effects term for each spatial unit ($i = I$) is a weighted sum across all latent factors k in 1 to n ($\dot{\lambda}_I^{\intercal} \dot{f}_t = \sum_{k=1}^{n} \lambda_{I,k} f_{k,t}$).

The model is fit to estimate the effects of the cyclone in each district over time ($\delta_{i,t}$) in three steps. First, observations from the control districts alone are used to estimate coefficients ($\dot{\beta}$) for the climate variables, latent factors ($\dot{f}$), and

factor loadings ($\dot{\lambda}$) for the control districts based on entire time series (including the post-cyclone period). Next, factor loadings are estimated for the cyclone-affected units such that the mean squared prediction error during the pre-cyclone period is minimized. Because the aim of the generalized synthetic control was to minimize prediction error with respect to cases, factor loadings were determined without any consideration of which control districts were matched to which cyclone-affected districts in the prior step. Finally, the effect of the cyclone on cases for a given cyclone-affected district i in each time period t following the cyclone (δ_{it}) is estimated as the difference between observed incidence and indicence predicted by the synthetic control ($\hat{Y_{i,t}}$):

$$\delta_{i,t} = Y_{i,t} - \hat{Y_{i,t}} = Y_{i,t} - \dot{x}_{i,t}^{\intercal}\dot{\beta} - \dot{\lambda}_i^{\intercal}\dot{f}_t$$

Analysis was conducted using the R package fect: Fixed Effects Counterfactual Estimators (Liu et al. 2022). The number of latent factors to use in the model was selected to minimize mean squared prediction error. For each number of latent factors from zero to five, ten rounds of cross-validation were conducted by withholding 10% of the control units when fitting the model and calculating the mean squared prediction error across the testing units. The number of latent factors that minimized the mean squared prediction error was then selected. Nonparametric confidence intervals for the proportion of cases attributable to the cyclone were calculated across 1000 bootstrap runs. We conducted sensitivity analyses to examine the effects of varying the number of latent factors (Figure 24) and excluding climate covariates from the model (Figure 15).

2.5 Examining associations between climate, vulnerability indices and cyclone-attributable incidence

We examine the relationship between cyclone-attributable dengue incidence rotated components that combine climate covariates with vulnerability indices related to housing quality and water access, all of which may moderate the effect of extreme precipitation on dengue. We took population-weighted averages of manzana (block)- level vulnerability indices across each district (see Table 5 for a full list and description of vulnerability indices). We also calculated average daily mean temperature and cumulative precipitation during Cyclone Yaku. We used the *psych* package in R to load the vulnerability indices across four principal components after determining that four principal components would best balance interpretability against capturing variation across the districts by optimizing very simple structure (VSS) complexity 1 (Revelle 2007). The principal components were rotated using Varimax rotation, which rotates the principal components so that they more strongly correlate with the variables of interest, improving interpretability (Keith E. Dilbeck 2017). Next, we fit a linear regression of the cyclone-attributable dengue incidence per thousand people in each district (summed from April 22nd - November 3rd, 2023) against the rotated components (RCs).

$$\delta_i = \alpha_1 RC_1 + \alpha_2 RC_2 + \alpha_3 RC_3 + \alpha_4 RC_4 + \gamma$$

We bootstrapped our estimates of the coefficients (α) and intercept (γ), incorporating uncertainty with respect to cyclone-attributable incidence, by sampling with replacement across districts and their corresponding distributions of cyclone-attributable incidence estimates, interactively fitting parameters and thereby estimating distributions of coefficient and intercept values. We also visually examined the relationship between cyclone-attributable cases and mean temperature during Cyclone Yaku.

2.6 Quantifying the influence of historical climate forcing on the probability of extreme March precipitation in northwestern Peru

To test whether historical climate forcing has significantly increased the likelihood of extreme precipitation in northwestern Peru, we analyzed climate model simulations from Phase 6 of the Coupled Model Intercomparison Project (CMIP6) database, which is archived by the Earth System Grid Federation and can be downloaded from their website at https://esgf-node.llnl.gov/search/cmip6/. To incorporate uncertainty arising from both differences in climate model structure and internal climate variability, we downloaded simulations from seven different climate models (ACCESS-ESM1-5, CanESM5, CNRM-CM6-1, IPSL-CM6A-LR, MIROC6, MIROC-ES2L, and NorCPM1) that archived at least 29 realizations in the CMIP6 historical forcing experiment (which spans 1850-2014). Our ensemble thus consists of a total of 203 simulations, each of which provides a unique realization of possible weather conditions that could have occurred during 1850-2014, consistent with the pathway of natural and anthropogenic emissions found in observational data. We then compared the likelihood of extreme monthly precipitation in March across simulations for three periods: 1850 - 1899 (preindustrial baseline), 1900 - 1964 (early historical), and 1964 - 2014 (late historical).

For each of these simulations, we extracted the March precipitation data and calculated the area-weighted average monthly precipitation values over northwestern Peru, defined as -3 N to -9 N and -82 E to -76 E (Figure 14). During Cyclone Yaku, March precipitation in cyclone-affected regions exceeded the 85th percentile of observations from 1973 - 2022 according to the population-weighted ERA5 precipitation data (Figure 6). To reflect these conditions, we define extreme precipitation as a month that exceeds the 85th percentile for monthly mean precipitation during the last 30 years of the historical forcing experiment (1985 - 2014). We calculated the 85th percentile precipitation threshold separately for each climate model to account for biases in the mean and standard deviation of precipitation across different models. To estimate changes in the frequency of extreme March precipitation, we calculated the percentage of simulations with extreme March conditions for each calendar year. We then conducted a Kolmogorov-Smirnov test to examine the likelihood that the prob-

ability distributions in each of the two respective later periods came from the same distribution as the preindustrial baseline. This null hypothesis reflects the assumption that extreme precipitation events would have been as likely in the early and late historical periods compared to the preindustrial baseline without historical anthropogenic emissions.

3 Results

3.1 Districts with the most anomalous precipitation during Cyclone Yaku generally had warm, dry climates

We defined cyclone-affected districts as those with precipitation anomalies exceeding 8.5 mm/day while the control pool was comprised of districts with precipitation anomalies below 7.0 mm/day, noting that the latter districts may still have experienced some impacts of Cyclone Yaku, although likely to a lesser extent. The cutoff of 8.5 mm/day corresponded to the 90th percentile of precipitation anomalies across districts reporting dengue in 2023, a threshold that both corresponded to an extreme value for precipitation anomalies during this time in Peru and ensured that a sufficient number of cyclone-unaffected districts could be included in the control pool Figure 7. There were 56 cyclone-affected districts predominantly located in the regions of Tumbes, Piura, and Lambayeque, which others have also identified as the regions that experienced the greatest impacts of Cyclone Yaku (Table 1, Figure 1B, Figure 7A) (SENAMHI 2023; MapAction). There were 463 districts with precipitation anomalies below 7.0 mm/day that reported dengue cases in 2023, which we designated as cyclone-unaffected (Figure 8). We additionally tested the sensitivity of the generalized synthetic control analysis to different thresholds for cyclone-affected and cyclone-unaffected districts (subsection 2.2).

Following matching, 194 districts predominantly in the eastern rainforest and the northern coast were included in the control pool (Figure 8). Matching selected for a set of districts that, on average, more closely reflected the relationship between temperature and precipitation in the cyclone-affected districts, where relatively hotter temperatures (exceeding 23°C) coincided with moderate to heavy precipitation (exceeding 3 mm/day) (Figure 9). Matching also eliminated periods of especially large imbalance with respect to precipitation between cyclone-affected and control districts (i.e., much heavier precipitation in the cyclone-unaffected districtsFigure 10A, B). However, the standardized difference between the cyclone-affected districts and the matched control districts repeatedly exceeded one standard deviation for both climate covariates (approximately 3°C and 4 mm/day of precipitation), indicating considerable remaining imbalance (Figure 10, see discussion in subsubsection 6.1.2).

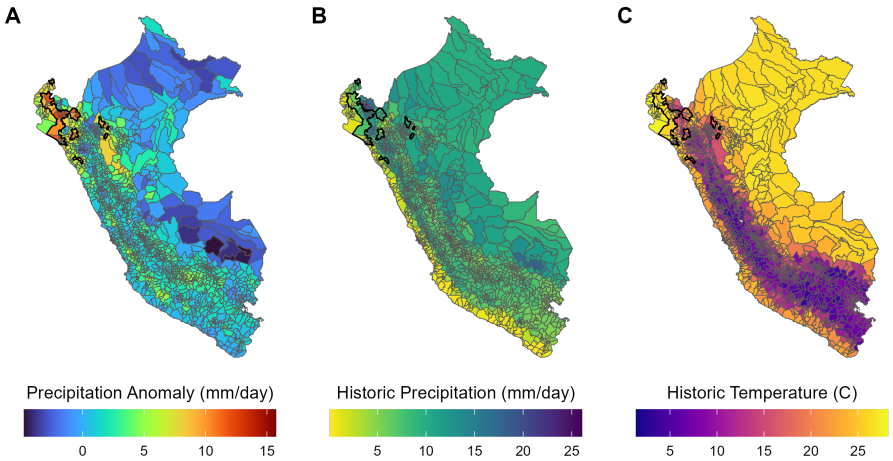

Figure 1: Historic climate conditions across districts in Peru compared to during Cyclone Yaku. In all panels, the bold outline encompasses districts included in cyclone-affected group. (A) Precipitation anomalies (mm/day), calculated as the difference between the mean daily precipitation between March 7-20, 2023 and the mean daily precipitation during the same time period across the reference years 1993 - 2022, excluding 2017. (B) Average daily precipitation (mm/day) across the historic reference period. (C) Average temperature (in degrees Celsius) across the historic reference period.

3.2 Cyclone Yaku caused 67% of dengue cases in the cyclone-affected districts

We estimated positive effects of both temperature and precipitation on cases (Table 3) . Models with five latent factors minimized prediction error during cross-validation (Figure 12; see Figure 13 for corresponding factor loadings). The generalized synthetic control model generally predicted cases well across cyclone-affected districts in the pre-cyclone period ($R^2 = 0.60$) (Figure 2A), including during the large outbreak in 2017.

Dengue cases were significantly elevated in cyclone-affected districts compared to the synthetic control ($p < 0.05$) for over six months (April 22nd - November 3rd). During that time period, 38,209 (95% confidence interval: 17,454 - 49,928) out of 57,246 total cases in cyclone-affected districts were attributable to Cyclone Yaku. In other words, 67% (95% confidence interval: 30% - 87%) of cases were attributable to the cyclone. The percentage of cases attributable to the cyclone was largely consistent across this six-month period, while the number of cyclone-attributable cases peaked between May 20th and June 16th, when 12,518 (95% confidence interval: 5,081 - 16,457) of cases were attributable to Cyclone Yaku (Figure 2B, Table 4).

Our main estimate of dengue cases attributable to Cyclone Yaku is robust. The percentage of cases attributable to the cyclone did not change substantially when climate covariates were excluded from the model or transformed, when the time series was extended to include observations prior to 2016, or when obser-

vations from the peak of the COVID-19 pandemic (2020 - 2021) were removed (Figure 15, Figure 17, Figure 19, Figure 20, Figure 21). The percentage of cases attributable to the cyclone was robust to changes in the threshold for cyclone-affected districts but varied and became more uncertain with changes in the threshold for cyclone-unaffected districts (Figure 22). We estimated a smaller percentage of cyclone-attributable cases (41%) when the control pool included only coastal districts (although these districts may have been partially affected by the cyclone, Figure 16) and a larger percentage of cyclone-attributable cases (97%) when we conducted the analysis at the region level rather than the finer district level (Figure 25). Estimates were generally robust to the number of control districts to which each cyclone-affected district was matched and to the number of latent factors included in the model (Figure 23, Figure 24).

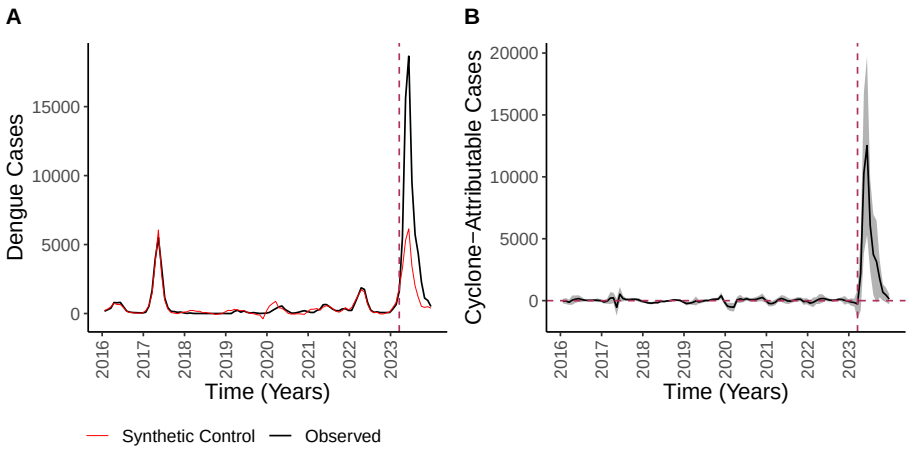

Figure 2: Main results of generalized synthetic control analysis across all control districts over time. (A) Total observed cases (black) across all cyclone-affected districts over time compared to the total cases in the synthetic control districts (red). (B) The difference between observed cases in the cyclone-affected districts versus in the synthetic controls over time, where the period after the dashed line indicates the effect of the cyclone. The grey ribbon corresponds to the 95% confidence interval. The dashed horizontal line indicates no effect and the dashed vertical line indicates when the cyclone occurred, meaning the only the difference in cases to the right of this vertical line is attributable to Cyclone Yaku.

3.3 Cyclone-attributable incidence varied with housing quality, hydrology, and temperature

There was considerable variation in the number of cyclone-attributable cases per thousand people across the cyclone-affected districts, with the greatest attributable incidence reported in Salitral, Piura (74.9 cyclone-attributable cases per thousand) (Figure 3). The northwestern regions of Tumbes, Piura, and Lambayeque that were most impacted by the cyclone had several districts where more than 20 cases of dengue per thousand people were caused by Cyclone Yaku

(Figure 3, Figure 7B). Cyclone-attributable incidence peaked several months earlier in cyclone-affected districts in Lambayeque and Piura compared to those in Tumbes and La Libertad. Cyclone Yaku did not have a large impact on dengue cases in cyclone-affected districts in San Martin and Cajamarca regions, which were both farther east.

A single cyclone-affected district (Lancones, Piura) was excluded from the following analysis of factors correlated with cyclone-attributable incidence because data on its vulnerability indices were unavailable. We summarized multivariate socio-environmental variation among districts using a principal components analysis with rotated components aimed at increasing interpretability. Each of the rotated components was strongly positively associated with one to two climate or vulnerability indices (standardized loading > 0.7): low-quality roofs and low-quality walls (RC_1), low-quality floors and precipitation during Cyclone Yaku (RC_2), temperature during Cyclone Yaku and flood risk (RC_3), and non-public water sources (RC_4). No components had strong negative associations (standardized loading $<$ -0.7). Based on the positive associations of cyclone-attributable cases with RC1 and RC3 ($p = 0.012$ and $p < 0.001$ respectively, Figure 4, Table 6), the largest cyclone-attributable dengue cases occurred in districts with greater proportions of low-quality roofs and walls, flood susceptibility, and warmer temperatures. Separate from the RCs, we find that significantly positive cyclone-attributable incidence only occurred in districts where mean temperature exceeded 24°C during Cyclone Yaku (Figure 4B).

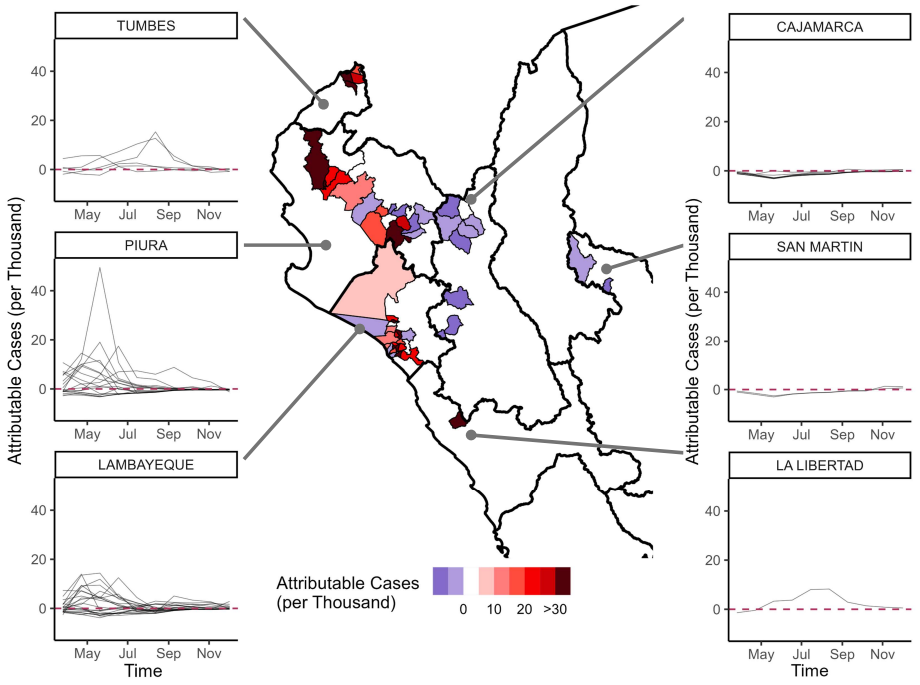

Figure 3: Spatial heterogeneity in the number of cyclone-attributable cases per thousand people. In the center, a map of the number of cyclone-attributable cases per thousand people across districts (calculated from April 22nd – November 3, 2023), zoomed into the region of Peru where the cyclone had the greatest impact. Each cyclone-affected district is outlined and shaded according to the estimated number of attributable cases, with darker red indicating a larger positive effect and blue indicating a negative effect. The dark outlines show borders of regions. The left and right columns of plots display cyclone-attributable dengue cases per thousand people over time following Cyclone Yaku (in the year 2023), with each facet corresponding to a different region. Grey lines connect faceted plots to their geographic location on the map and the top label gives the region name. Within the faceted plots, each line corresponds to a different cyclone-affected district within the region and the horizontal dashed red lines indicate the baseline of zero cyclone-attributable cases.

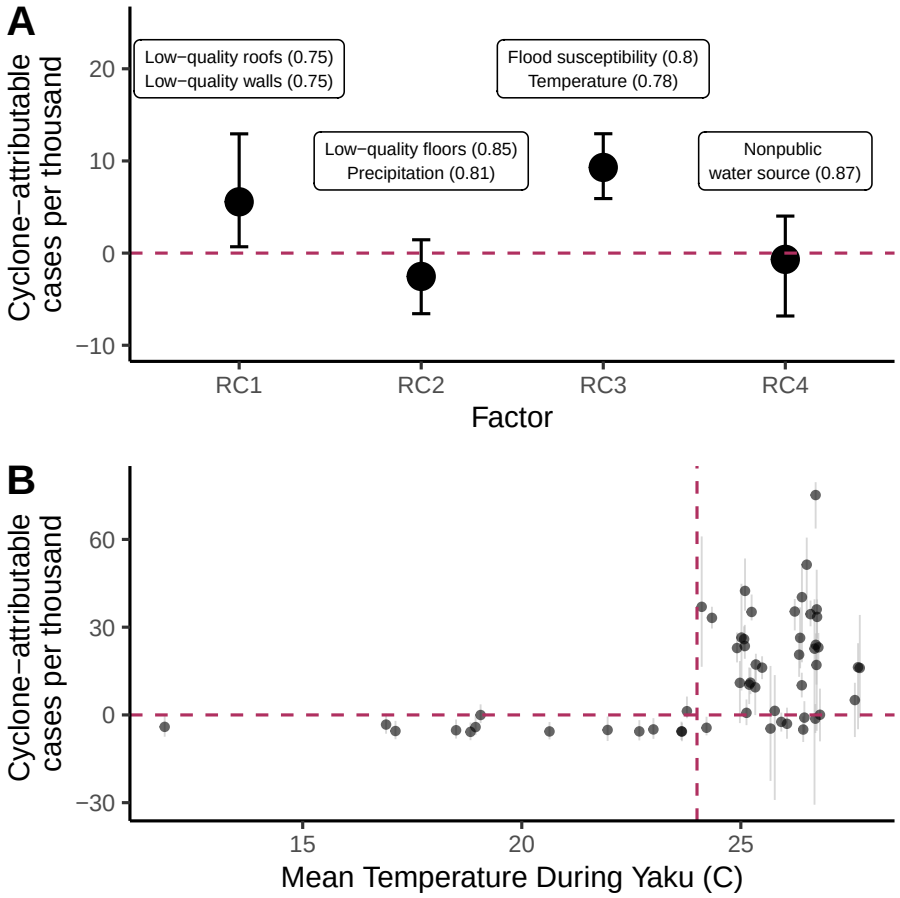

Figure 4: The number of cyclone-attributable cases per thousand people varies across districts with hydrological factors, housing quality, and mean temperature. (A) Estimates and 95% confidence intervals for the association between vulnerability indices (rotated components, RCs) and cyclone-attributable cases per thousand people at the district level from April 22nd - November 3, 2023. Labels at the top of the plot give the names of the variables most strongly associated with each rotated component ($|$ standardized loading $| > 0.7$) (see Table 5). The standardized loading is given in parentheses (where $|$ standardized loading $| = 1$ is the strongest possible association). (B) The number of cyclone-attributable cases per thousand people (April 22nd - November 3, 2023) is plotted for each district with 95% confidence intervals against the mean temperature in that district during Cyclone Yaku. The red horizontal line indicates no effect of Cyclone Yaku on cases, while the red vertical line indicates 24°C.

3.4 Extreme precipitation in March in northwestern Peru is 42% more likely due to historical climate forcing

Climate model simulations of the historical period (1850-2014) suggest that anthropogenic emissions have increased the likelihood of extreme monthly precipitation during the month of March over northwestern Peru. Across an ensemble of 203 total realizations from 7 different climate models, we find that 10.76% of the simulated March precipitation values from the 1850-1899 period were extreme. The frequency increased to 13.00% in the early historical period (1900-1964) and to 15.30% in the late historical period (1965-2014). In other words, extreme precipitation events were 21% more likely in the early historical period and 42% more likely in the late historical period compared to the preindustrial baseline. Based on the Kolmogorov-Smirnov test, the frequency of extreme precipitation events is significantly higher across both the early and late historical periods compared to the pre-industrial period ($p < 0.001$ for both, Figure 5). The frequency of extreme precipitation events also increased significantly by 18% from the early to late historical periods ($p = 0.011$).

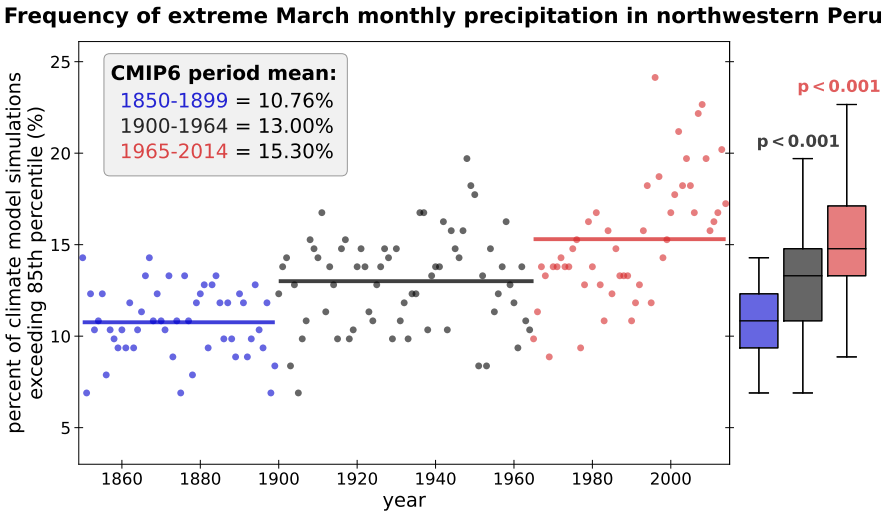

Figure 5: The frequency of extreme March monthly precipitation values in northwestern Peru has increased significantly compared to the pre-industrial baseline. Annual values show the percentage of 203 climate model simulations exhibiting extreme March precipitation during each calendar year of the CMIP6 historical forcing experiment, which is available from 1850 to 2014. The percentage of climate model simulations is calculated from the 7 climate models that have archived at least 29 realizations in the CMIP6 historical forcing experiment, generating an ensemble of 203 realizations. Based on the precipitation quantiles associated with Cyclone Yaku (see Methods), extreme monthly precipitation is defined to have occurred when the March monthly precipitation averaged over northwestern Peru exceeds the 85th percentile threshold for the recent climate (calculated from the last 30 years of the CMIP6 historical forcing experiment, or 1985-2014). Solid lines show the mean frequency for the preindustrial (1850-1899, blue), early historical (1900-1964, gray), and late historical (1965-2014, red) periods. Boxplots show the distribution of annual values for each time period. P-values show the probability that the distributions for 1900-1964 and 1965-2014 come from the same distribution as 1850-1899 using a Kolmogorov-Smirnov Test.

4 Discussion

Anthropogenic climate change is increasing the likelihood and intensity of extreme weather events, which may in turn trigger outbreaks of infectious diseases (Alcayna et al. 2022; Mora et al. 2022). Here, we conducted one of the first analyses to connect a climate attribution analysis with a causal assessment of how much a particular extreme weather event contributed to an infectious disease outbreak (Carlson et al. 2024; Ebi and Hess 2020). Across six months, 38,209 (95% CI: 17,454 - 49,928) dengue cases were attributable to Cyclone Yaku in the 56 districts of Peru with the greatest precipitation anomalies (Figure 2). For the cyclone-affected districts, this corresponds to 67 (95% CI: 30 - 87) % of reported cases and 17.8 (95% CI: 8.1 - 23.3) cyclone-attributable cases per thousand peo-

ple. Further, we find that extreme monthly precipitation during March like that associated with Cyclone Yaku has become 42% more likely in northwestern Peru because of climate forcing since the preindustrial era (Figure 5).

This work demonstrates how synthetic control methods, which have already been used in similar epidemiological context (Sheridan et al. 2022; Schwarz et al. 2023; Bruhn et al. 2017; Shioda et al. 2021; Nyathi et al. 2019; Jones et al. 2020), can facilitate causal estimates of the effects of extreme weather on infectious disease. Using interactive fixed effects, we controlled for the effects of confounders that vary across time and space and may not be readily measured or may influence dengue transmission in ways that are not well-understood (e.g., immunity, vector control, mobility, and strain type), a notable methodological advance given that studies focused on dengue have often been limited by their inability to account for important covariates (Laureano-Rosario et al. 2017; Minh An and Rocklöv 2014; Giesen et al. 2020). Although the COVID-19 pandemic likely disrupted dengue dynamics through its impacts on health systems and human behavior, we found no effect of excluding the years 2020 - 2021 from the model, which suggests that our estimates are robust (Brady and Wilder-Smith 2021; Chen et al. 2022). Substantial imbalance with respect to baseline climate remained between the cyclone-affected and cyclone-unaffected districts after matching (Figure 11 ,Figure 10). However, matching generally selected for districts where warmer temperatures coincided with more intense precipitation (reflecting conditions that may favor larger dengue outbreaks) (Figure 9) and improved the fit of the model to actual cases (Figure 23). Given the positive association between both mean precipitation and mean temperature and cases (Table 3), comparing the cyclone-affected districts to a set of cyclone-unaffected districts that tended to be more warm and wet on average (Table 2, Figure 11) biases us toward underestimating the effects of Cyclone Yaku on cases. We were able to further control for weather factors that were not caused by the cyclone (e.g., coastal El Niño conditions) both by including temperature and precipitation as covariates in the model and by including coastal districts affected by the coastal El Niño in the control pool. These adjustments also likely cause us to underestimate the true of extent to which precipitation anomalies contributed to Peru's outbreak, both because the model removes the estimated linear effect of rainfall on dengue cases and because we intentionally exclude coastal El Niño effects (Figure 15). In other words, our estimated effect captures the effects of Cyclone Yaku (as defined by precipitation anomalies) on dengue cases above and beyond the linear effects of increased rainfall and suitable temperature and the effects of El Niño. This makes even our large estimate of cyclone-attributable dengue cases conservative.

While this study adds to the body of work linking epidemics to cyclones and other extreme events (Alcayna et al. 2022; Mora et al. 2022; Ivers and Ryan 2006), it is important to note that this connection is neither ubiquitous nor inevitable. Vector-borne disease outbreaks are only possible when extreme weather events occur in environments that can facilitate sustained transmission, which timely interventions may preclude. Instances where extreme weather appeared to have little or no effect on transmission may be instructive both for

forecasting epidemics and identifying effective preventative measures to apply following of extreme events (Beatty et al. 2007; Nosrat et al. 2021). The effects of Cyclone Yaku on dengue incidence varied across districts, a result that may help clarify risk factors associated with large outbreaks after extreme precipitation (Figure 3). In particular, districts with poor housing quality (i.e., residences built with low-quality roof and wall materials) tended to have higher cyclone-attributable dengue incidence (Figure 4A), a result consistent with our hypothesis that such dwellings increase human contact with mosquitoes and experience more damage following an extreme weather event (Mulligan et al. 2015; Borbor-Cordova et al. 2020). Importantly, this analysis does not necessarily imply that low-quality roofs and walls are the most important covariates compared to other vulnerability indices. Rather, our model only considered a set of rotated factors that best captured the differences in measured covariates between districts, meaning that other potentially important variables that may be associated with outbreak risk but were not measured or were highly correlated with other variables were not analyzed. However, dengue exposure and disease risk is associated with many social determinants of health such as reduced access to healthcare, water insecurity, and poverty (Carabali et al. 2015; Vincenti-Gonzalez et al. 2017). Efforts to improve infrastructure and reduce social inequalities may reduce vulnerability to both extreme weather and vector-borne disease (Gibb et al. 2023; Mulligan et al. 2015). Further, expanded testing in under-resourced and crisis settings remains critical, as biases in epidemiological data could lead to uneven and incomplete estimates of the true health costs of extreme weather (Kakkar 2012; Clarke et al. 2024).

We did not detect a significant linear association between cyclone-attributable dengue incidence and absolute precipitation, which may be because our model explicitly accounts for a linear effect of precipitation on cases, or may reflect the nonlinear and complicated relationship between precipitation and dengue risk (Figure 4A). Heavy rainfall can create vector breeding habitat, but excessive precipitation may flush out larvae and reduce vector abundance (Shocket et al. 2020; Caldwell et al. 2021; Lowe et al. 2018). Methods have not yet been developed for studying continuous treatment effects using generalized synthetic controls and directly estimating exposure-response relationships. Therefore, we defined cyclone-affected units using a relatively conservative threshold of precipitation anomalies greater than 8.5 mm/day to ensure a sufficiently large control pool. However, the proportion of cases that were cyclone attributable was approximately equivalent (68%; 95% confidence interval: 45% - 83%) in a sensitivity analysis using a lower threshold of 7 mm/day (Figure 22), meaning that our analysis likely underestimates the total number of cyclone-attributable dengue cases by excluding impacted districts from the cyclone-affected pool. These methods may be applied to other instances when extreme weather preceded infectious disease outbreaks to help identify the threshold at which anomalous precipitation can trigger outbreaks and examine how the characteristics of a weather events (e.g., wind speed, total rainfall, and event duration) relate to its impact on transmission.

Warmer districts with greater flood risk (defined by topographic features

and vegetation cover) also had greater cyclone-attributable dengue incidence (Figure 4A), suggesting that the relationship between dengue and extreme precipitation is context-dependent. Anomalous precipitation poses the greatest risk in settings where environmental factors promote flooding, which can create vector breeding habitat, disrupt water and wastewater services, displace residents, and impede vector control efforts (Lowe et al. 2018; Coalson et al. 2021). The co-occurrence of Cyclone Yaku with warmer temperatures that are suitable for transmission by *Aedes aegypti* may have exacerbated outbreak risk (Mordecai et al. 2019). Significant increases in dengue due to Cyclone Yaku were only observed in districts where mean temperature exceeded 24°C during Cyclone Yaku (Figure 4B). Further analysis across multiple extreme events may determine whether outbreak size is proportional to temperature-dependent transmission risk inferred from mosquito biology or whether outbreak size is largely independent of temperature within a certain range across which outbreaks can be sustained (Skaff et al. 2020; Caldwell et al. 2021). Although March of 2023 was not an anomalously hot period in northwestern Peru, warming has likely increased the likelihood that extreme precipitation will co-occur with suitable temperature conditions. Indeed, historical and future warming are expected to increase dengue burden in many parts of the world by increasing temperatures toward the thermal optimum for dengue transmission of 29°C (estimated by Mordecai et al. (2019), see Figure 18) (Giesen et al. 2020; Colón-González et al. 2021; Messina et al. 2019). Historical warming is estimated to have caused a relatively large share of dengue cases in Peru compared to other countries, suggesting that anthropogenic climate change has disproportionately exacerbated dengue burden in Peru (Childs et al. 2024), both through warming and more frequent extreme precipitation events.

Extremely high monthly precipitation in March, like that associated with Cyclone Yaku, are significantly more likely in northwestern Peru in the present-day climate (relative to the 1850-1899 preindustrial baseline) as a result of historical climate forcing (Figure 5). Our estimate of a 42% increase in likelihood is consistent with a prior attribution analysis, which found that anthropogenic forcing increased the likelihood of extreme rainfall across Peru in March of 2017 by 50% during similar coastal El Niño events (Christidis et al. 2019). Although our attribution analysis was generally designed to analyze the influence of anthropogenic forcing on precipitation intensity for districts heavily impacts by Cyclone Yaku (Figure 6), we average our results over a broader region of Northwest Peru through the entire month of March to avoid issues caused by the limited spatial and temporal resolution of available CMIP6 model simulations. Since CMIP6 simulations using observed historical climate forcings only extend to 2014, we use the period 1965-2014 as an estimate of the present-day climate. The fact that greenhouse gas emissions and global warming continued over the subsequent decade make this a conservative choice. We note that the CMIP6 climate models are somewhat limited in their ability to realistically simulate extreme precipitation (Donat et al. 2023). Since fine-scale processes can modify extreme event risk (Diffenbaugh et al. 2005), the causal contribution of anthropogenic forcing to precipitation intensity during Cyclone Yaku may be studied

more precisely using a high-resolution storyline attribution approach that incorporates the specific atmospheric conditions leading up to this event (e.g., Reed and Wehner (2023)). Still, the two-part analysis presented here is an important step in investigating the linkages between climate change and human health. We found that anthropogenic forcing has likely increased the risk of extremely wet conditions like those associated with Cyclone Yaku, which in turn caused the majority of dengue cases during an unprecedented dengue outbreak in Peru (Ebi et al. 2020; Hegerl et al. 2010; Carlson et al. 2024).

Comprehensive assessments of the benefits of reducing greenhouse gas emissions and the scope of loss and damages from existing climate change are necessary to guide climate justice efforts and inform planning for future climate scenarios (Scovronick et al. 2019). Studies like ours build understanding of the health costs of climate change, particularly the connections between climate change-driven extreme weather and infectious diseases, which are understudied (Ebi and Hess 2020; Carlson et al. 2024). Many projections of dengue burden under climate change focus only on trends in endemic areas due to long-term changes in mean temperature, often neglecting to incorporate changes in precipitation altogether (Childs et al. 2024; Ryan et al. 2019). Impacts of precipitation on mosquito biology are also relatively complex, context-dependent, and less well-understood compared to those of temperature (Shocket et al. 2020). However, capturing the extent to which disease burden will increase with climate change requires models that are capable of forecasting large outbreaks driven by extreme weather, as well as enhanced disease surveillance and meteorological monitoring in sites vulnerable to large epidemics of climate-sensitive disease. Understanding the connection between climate change and dengue may also offer new opportunities for proactive dengue prevention activities. Dengue control policy often centers on technical, localized interventions that, while critical, are typically costly, short-term, and deployed reactively (Espinoza 2021; The Lancet Infectious Diseases 2023). Given the connections that we have demonstrated between historical human activity and the type of extreme precipitation event that can drive large dengue epidemics, mitigating further global warming and building climate-resilient infrastructure may help prevent epidemics and protect human health against further increases in dengue risk (Childs et al. 2024).

Acknowledgements

This project was made possible by Peru's Program Investigando con el CDC (Investigating with the CDC Program). We are grateful to CDC Peru for the opportunities they provide to students through this program. We additionally thank Raisa Paredes for supporting this collaboration. We thank Kelsey Pano Lyberger for her assistance with obtaining case data for Mexico, Brazil, and Colombia. We thank Marissa Childs for her assistance with extracting climate data from Google Earth Engine. We appreciate the guidance and assistance provided by Yiqing Xu on generalized synthetic control models and the fect package. We also thank Nathan Lo and Andrew MacDonald for their insights on applying synthetic control methods. We would wish to acknowledge computational resources from Google Cloud for Earth Engine and thank Michael Sherman for his assistance applying for additional batch task quota through the uplift program. We acknowledge the World Climate Research Programme, which, through its Working Group on Coupled Modelling, coordinated and promoted CMIP6. We thank the climate modeling groups for producing and making available their model output, the Earth System Grid Federation (ESGF) for archiving the data and providing access, and the multiple funding agencies who support CMIP6 and ESGF.

MJH was supported by the Achievement Rewards for College Scientists Scholarship and the National Institutes of Health (R35GM133439). EAM was supported by the National Institutes of Health (R35GM133439, R01AI168097, R01AI102918), the National Science Foundation (DEB-2011147, with Fogarty International Center), and the Stanford Center for Innovation in Global Health, King Center on Global Development, and Woods Institute for the Environment. AGL was supported by the National Institutes of Health (D43TW007393, with Fogarty International Center). NSD and JTT acknowledge support from Stanford University.

5 Works Cited

References

A. Adeola, J. Botai, H. Rautenbach, O. Adisa, K. Ncongwane, C. Botai, and T. Adebayo-Ojo. Climatic Variables and Malaria Morbidity in Mutale Local Municipality, South Africa: A 19-Year Data Analysis. *International Journal of Environmental Research and Public Health*, 14(11):1360, Nov. 2017. ISSN 1660-4601. doi: 10.3390/ijerph14111360. URL http://www.mdpi.com/1660-4601/14/11/1360.

T. Alcayna, I. Fletcher, R. Gibb, L. Tremblay, S. Funk, B. Rao, and R. Lowe. Climate-sensitive disease outbreaks in the aftermath of extreme climatic events: A scoping review. *One Earth*, 5(4):336–350, Apr. 2022.

ISSN 2590-3322. doi: 10.1016/j.oneear.2022.03.011. URL https://www.sciencedirect.com/science/article/pii/S2590332222001440.

S. Bagcchi. Dengue outbreak in Peru affects adults and children. *The Lancet Infectious Diseases*, 23(9):e339, Sept. 2023. ISSN 1473-3099, 1474-4457. doi: 10.1016/S1473-3099(23)00229-3. URL https://www.thelancet.com/journals/laninf/article/PIIS1473-3099(23)00229-3/fulltext. Publisher: Elsevier.

M. E. Beatty, E. Hunsperger, E. Long, J. Schürch, S. Jain, R. Colindres, G. Lerebours, Y.-M. Bernard, J. G. Dobbins, M. Brown, and G. G. Clark. Mosquitoborne Infections after Hurricane Jeanne, Haiti, 2004. *Emerging Infectious Diseases*, 13(2):308–310, Feb. 2007. ISSN 1080-6040, 1080-6059. doi: 10.3201/eid1302.061134. URL http://wwwnc.cdc.gov/eid/article/13/2/06-1132_article.htm.

M. J. Borbor-Cordova, G. Ger, A. A. Valdiviezo-Ajila, M. Arias-Hidalgo, D. Matamoros, I. Nolivos, G. Menoscal-Aldas, F. Valle, A. Pezzoli, and M. D. P. Cornejo-Rodriguez. An Operational Framework for Urban Vulnerability to Floods in the Guayas Estuary Region: The Duran Case Study. *Sustainability*, 12(24):10292, Dec. 2020. ISSN 2071-1050. doi: 10.3390/su122410292. URL https://www.mdpi.com/2071-1050/12/24/10292.

O. Brady and A. Wilder-Smith. What Is the Impact of Lockdowns on Dengue? *Current Infectious Disease Reports*, 23(2):2, Feb. 2021. ISSN 1523-3847, 1534-3146. doi: 10.1007/s11908-020-00744-9. URL https://link.springer.com/10.1007/s11908-020-00744-9.

C. A. W. Bruhn, S. Hetterich, C. Schuck-Paim, E. Kürüm, R. J. Taylor, R. Lustig, E. D. Shapiro, J. L. Warren, L. Simonsen, and D. M. Weinberger. Estimating the population-level impact of vaccines using synthetic controls. *Proceedings of the National Academy of Sciences*, 114(7):1524–1529, Feb. 2017. ISSN 0027-8424, 1091-6490. doi: 10.1073/pnas.1612833114. URL https://pnas.org/doi/full/10.1073/pnas.1612833114.

M. Burger, J. Wentz, and R. Horton. The Law and Science of Climate Change Attribution. *Columbia Journal of Environmental Law*, page Vol. 45 No. 1 (2020): Volume 45.1, Feb. 2020. doi: 10.7916/CJEL.V45I1.4730. URL https://journals.library.columbia.edu/index.php/cjel/article/view/4730.

J. M. Caldwell, A. D. LaBeaud, E. F. Lambin, A. M. Stewart-Ibarra, B. A. Ndenga, F. M. Mutuku, A. R. Krystosik, E. B. Ayala, A. Anyamba, M. J. Borbor-Cordova, R. Damoah, E. N. Grossi-Soyster, F. H. Heras, H. N. Ngugi, S. J. Ryan, M. M. Shah, R. Sippy, and E. A. Mordecai. Climate predicts geographic and temporal variation in mosquito-borne disease dynamics on two continents. *Nature Communications*, 12(1):1233, Feb. 2021. ISSN 2041-1723. doi: 10.1038/s41467-021-21496-7. URL https://www.nature.com/

articles/s41467-021-21496-7. Number: 1 Publisher: Nature Publishing Group.

M. Carabali, L. M. Hernandez, M. J. Arauz, L. A. Villar, and V. Ridde. Why are people with dengue dying? A scoping review of determinants for dengue mortality. *BMC Infectious Diseases*, 15(1):301, Dec. 2015. ISSN 1471-2334. doi: 10.1186/s12879-015-1058-x. URL http://bmcinfectdis.biomedcentral.com/articles/10.1186/s12879-015-1058-x.

C. J. Carlson, T. A. Carleton, R. C. Odoulami, and C. H. Trisos. The historical fingerprint and future impact of climate change on childhood malaria in Africa, July 2023. URL https://www.medrxiv.org/content/10.1101/2023.07.16.23292713v1. Pages: 2023.07.16.23292713.

C. J. Carlson, D. Mitchell, R. Gibb, R. F. Stuart-Smith, T. Carleton, T. E. Lavelle, C. A. Lippi, M. Lukas-Sithole, M. A. North, S. J. Ryan, D. S. Shumba, M. Chersich, M. New, and C. H. Trisos. Health losses attributable to anthropogenic climate change, Aug. 2024. URL http://medrxiv.org/lookup/doi/10.1101/2024.08.07.24311640.

S. S. Chand, K. J. E. Walsh, S. J. Camargo, J. P. Kossin, K. J. Tory, M. F. Wehner, J. C. L. Chan, P. J. Klotzbach, A. J. Dowdy, S. S. Bell, H. A. Ramsay, and H. Murakami. Declining tropical cyclone frequency under global warming. *Nature Climate Change*, 12(7):655–661, July 2022. ISSN 1758-678X, 1758-6798. doi: 10.1038/s41558-022-01388-4. URL https://www.nature.com/articles/s41558-022-01388-4.

S. Chapman, C. E. Birch, J. H. Marsham, C. Part, S. Hajat, M. F. Chersich, K. L. Ebi, S. Luchters, B. Nakstad, and S. Kovats. Past and projected climate change impacts on heat-related child mortality in Africa. *Environmental Research Letters*, 17(7):074028, July 2022. ISSN 1748-9326. doi: 10.1088/1748-9326/ac7ac5. URL https://dx.doi.org/10.1088/1748-9326/ac7ac5. Publisher: IOP Publishing.

Y. Chen, N. Li, J. Lourenço, L. Wang, B. Cazelles, L. Dong, B. Li, Y. Liu, M. Jit, N. I. Bosse, S. Abbott, R. Velayudhan, A. Wilder-Smith, H. Tian, O. J. Brady, S. R. Procter, K. L. Wong, J. Hellewell, N. G. Davies, C. I. Jarvis, C. V. McCarthy, G. Medley, S. R. Meakin, A. Rosello, E. Finch, R. Lowe, C. A. B. Pearson, S. Clifford, B. J. Quilty, S. Flasche, H. P. Gibbs, L. A. C. Chapman, K. E. Atkins, D. Hodgson, R. C. Barnard, T. W. Russell, P. Klepac, Y. Jafari, R. M. Eggo, P. Mee, M. Quaife, A. Endo, S. Funk, S. Hué, A. J. Kucharski, W. J. Edmunds, K. O'Reilly, R. Pung, C. J. Villabona-Arenas, A. Gimma, K. Abbas, K. Prem, G. M. Knight, F. Y. Sun, W. Waites, J. D. Munday, M. Koltai, F. G. Sandmann, and D. C. Tully. Measuring the effects of COVID-19-related disruption on dengue transmission in southeast Asia and Latin America: a statistical modelling study. *The Lancet Infectious Diseases*, 22(5):657–667, May 2022. ISSN 14733099. doi: 10.1016/S1473-3099(22)00025-1. URL https://linkinghub.elsevier.com/retrieve/pii/S1473309922000251.

M. L. Childs, K. Lyberger, M. Harris, M. Burke, and E. A. Mordecai. Climate warming is expanding dengue burden in the Americas and Asia. preprint, Infectious Diseases (except HIV/AIDS), Jan. 2024. URL http://medrxiv.org/lookup/doi/10.1101/2024.01.08.24301015.

G. Chowell, B. Cazelles, H. Broutin, and C. V. Munayco. The influence of geographic and climate factors on the timing of dengue epidemics in Perú, 1994-2008. *BMC Infectious Diseases*, 11(1):164, Dec. 2011. ISSN 1471-2334. doi: 10.1186/1471-2334-11-164. URL https://bmcinfectdis.biomedcentral.com/articles/10.1186/1471-2334-11-164.

N. Christidis, R. A. Betts, and P. A. Stott. The Extremely Wet March of 2017 in Peru. *Bulletin of the American Meteorological Society*, 100(1):S31–S35, Jan. 2019. ISSN 0003-0007, 1520-0477. doi: 10.1175/BAMS-D-18-0110.1. URL https://journals.ametsoc.org/view/journals/bams/100/1/bams-d-18-0110.1.xml.

J. Clarke, A. Lim, P. Gupte, D. M. Pigott, W. G. Van Panhuis, and O. J. Brady. A global dataset of publicly available dengue case count data. *Scientific Data*, 11(1):296, Mar. 2024. ISSN 2052-4463. doi: 10.1038/s41597-024-03120-7. URL https://www.nature.com/articles/s41597-024-03120-7.

J. E. Coalson, E. J. Anderson, E. M. Santos, V. Madera Garcia, J. K. Romine, J. K. Luzingu, B. Dominguez, D. M. Richard, A. C. Little, M. H. Hayden, and K. C. Ernst. The Complex Epidemiological Relationship between Flooding Events and Human Outbreaks of Mosquito-Borne Diseases: A Scoping Review. *Environmental Health Perspectives*, 129(9):096002, Sept. 2021. ISSN 0091-6765, 1552-9924. doi: 10.1289/EHP8887. URL https://ehp.niehs.nih.gov/doi/10.1289/EHP8887.

F. J. Colón-González, M. O. Sewe, A. M. Tompkins, H. Sjödin, A. Casallas, J. Rocklöv, C. Caminade, and R. Lowe. Projecting the risk of mosquito-borne diseases in a warmer and more populated world: a multi-model, multi-scenario intercomparison modelling study. *The Lancet Planetary Health*, 5(7):e404–e414, July 2021. ISSN 25425196. doi: 10.1016/S2542-5196(21)00132-7. URL https://linkinghub.elsevier.com/retrieve/pii/S2542519621001327.

Copernicus Climate Change Service (C3S). ERA5: Fifth generation of ECMWF atmospheric reanalyses of the global climate., 2017. Published: Copernicus Climate Change Service Climate Data Store (CDS), https://cds.climate.copernicus.eu/cdsapp#!/home.

N. S. Diffenbaugh, J. S. Pal, R. J. Trapp, and F. Giorgi. Fine-scale processes regulate the response of extreme events to global climate change. *Proceedings of the National Academy of Sciences*, 102(44):15774–15778, Nov. 2005. ISSN 0027-8424, 1091-6490. doi: 10.1073/pnas.0506042102. URL https://pnas.org/doi/full/10.1073/pnas.0506042102.

N. S. Diffenbaugh, D. L. Swain, and D. Touma. Anthropogenic warming has increased drought risk in California. *Proceedings of the National Academy of Sciences*, 112(13):3931–3936, Mar. 2015. ISSN 0027-8424, 1091-6490. doi: 10.1073/pnas.1422385112. URL https://pnas.org/doi/full/10.1073/pnas.1422385112.

N. S. Diffenbaugh, D. Singh, J. S. Mankin, D. E. Horton, D. L. Swain, D. Touma, A. Charland, Y. Liu, M. Haugen, M. Tsiang, and B. Rajaratnam. Quantifying the influence of global warming on unprecedented extreme climate events. *Proceedings of the National Academy of Sciences*, 114(19):4881–4886, May 2017. ISSN 0027-8424, 1091-6490. doi: 10.1073/pnas.1618082114. URL https://pnas.org/doi/full/10.1073/pnas.1618082114.

M. G. Donat, C. Delgado-Torres, P. De Luca, R. Mahmood, P. Ortega, and F. J. Doblas-Reyes. How Credibly Do CMIP6 Simulations Capture Historical Mean and Extreme Precipitation Changes? *Geophysical Research Letters*, 50(14):e2022GL102466, July 2023. ISSN 0094-8276, 1944-8007. doi: 10.1029/2022GL102466. URL https://agupubs.onlinelibrary.wiley.com/doi/10.1029/2022GL102466.

K. L. Ebi and J. J. Hess. Health Risks Due To Climate Change: Inequity In Causes And Consequences: Study examines health risks due to climate change. *Health Affairs*, 39(12):2056–2062, Dec. 2020. ISSN 0278-2715, 1544-5208. doi: 10.1377/hlthaff.2020.01125. URL http://www.healthaffairs.org/doi/10.1377/hlthaff.2020.01125.

K. L. Ebi, C. Åström, C. J. Boyer, L. J. Harrington, J. J. Hess, Y. Honda, E. Kazura, R. F. Stuart-Smith, and F. E. L. Otto. Using Detection And Attribution To Quantify How Climate Change Is Affecting Health. *Health Affairs*, 39(12):2168–2174, Dec. 2020. ISSN 0278-2715. doi: 10.1377/hlthaff.2020.01004. URL https://www.healthaffairs.org/doi/full/10.1377/hlthaff.2020.01004.

R. Edwards, M. Bondarenko, A. Tatem, and A. Sorichetta. Unconstrained national Population Weighted Density in 2000, 2005, 2010, 2015 and 2020 (1km resolution), 2021. URL https://www.worldpop.org/doi/10.5258/SOTON/WP00702.

K. Emanuel. Assessing the present and future probability of Hurricane Harvey's rainfall. *Proceedings of the National Academy of Sciences*, 114(48):12681–12684, Nov. 2017. ISSN 0027-8424, 1091-6490. doi: 10.1073/pnas.1716222114. URL https://pnas.org/doi/full/10.1073/pnas.1716222114.

M. I. Espinoza. Conflicting diagnostic and prognostic framing of epidemics? Newspaper representations of dengue as a public health problem in Peru. *Social Science & Medicine*, 289:114398, Nov. 2021. ISSN 02779536. doi: 10.1016/j.socscimed.2021.114398. URL https://linkinghub.elsevier.com/retrieve/pii/S0277953621007309.

S. E. Fick and R. J. Hijmans. WorldClim 2: new 1-km spatial resolution climate surfaces for global land areas. *International Journal of Climatology*, 37(12): 4302–4315, Oct. 2017. ISSN 0899-8418, 1097-0088. doi: 10.1002/joc.5086. URL https://onlinelibrary.wiley.com/doi/10.1002/joc.5086.

R. Gibb, F. J. Colón-González, P. T. Lan, P. T. Huong, V. S. Nam, V. T. Duoc, D. T. Hung, N. T. Dong, V. C. Chien, L. T. T. Trang, D. Kien Quoc, T. M. Hoa, N. H. Tai, T. T. Hang, G. Tsarouchi, E. Ainscoe, Q. Harpham, B. Hofmann, D. Lumbroso, O. J. Brady, and R. Lowe. Interactions between climate change, urban infrastructure and mobility are driving dengue emergence in Vietnam. *Nature Communications*, 14(1):8179, Dec. 2023. ISSN 2041-1723. doi: 10.1038/s41467-023-43954-0. URL https://www.nature.com/articles/s41467-023-43954-0.

C. Giesen, J. Roche, L. Redondo-Bravo, C. Ruiz-Huerta, D. Gomez-Barroso, A. Benito, and Z. Herrador. The impact of climate change on mosquito-borne diseases in Africa. *Pathogens and Global Health*, 114(6):287–301, Aug. 2020. ISSN 2047-7724, 2047-7732. doi: 10.1080/20477724.2020.1783865. URL https://www.tandfonline.com/doi/full/10.1080/20477724.2020.1783865.

G. C. Hegerl, O. Hoegh-Guldberg, G. Casassa, M. Hoerling, S. Kovats, C. Parmesan, D. Pierce, and P. Stott. Good practice guidance paper on detection and attribution related to anthropogenic climate change. pages 1–8. Intergovernmental Panel on Climate Change (IPCC) Working Group, Jan. 2010. URL https://espace.library.uq.edu.au/view/UQ:236549.

K. Imai, I. S. Kim, and E. H. Wang. Matching Methods for Causal Inference with Time-Series Cross-Sectional Data. *American Journal of Political Science*, 67 (3):587–605, July 2023. ISSN 0092-5853, 1540-5907. doi: 10.1111/ajps.12685. URL https://onlinelibrary.wiley.com/doi/10.1111/ajps.12685.

L. C. Ivers and E. T. Ryan. Infectious diseases of severe weather-related and flood-related natural disasters. *Current Opinion in Infectious Diseases*, 19(5): 408–414, Oct. 2006. ISSN 0951-7375. doi: 10.1097/01.qco.0000244044.85393.9e. URL https://journals.lww.com/00001432-200610000-00003.

I. J. Jones, A. J. MacDonald, S. R. Hopkins, A. J. Lund, Z. Y.-C. Liu, N. I. Fawzi, M. P. Purba, K. Fankhauser, A. J. Chamberlin, M. Nirmala, A. G. Blundell, A. Emerson, J. Jennings, L. Gaffikin, M. Barry, D. Lopez-Carr, K. Webb, G. A. De Leo, and S. H. Sokolow. Improving rural health care reduces illegal logging and conserves carbon in a tropical forest. *Proceedings of the National Academy of Sciences*, 117(45):28515–28524, Nov. 2020. ISSN 0027-8424, 1091-6490. doi: 10.1073/pnas.2009240117. URL https://pnas.org/doi/full/10.1073/pnas.2009240117.

M. Kakkar. Dengue fever is massively under-reported in India, hampering our response. *BMJ*, 345(dec19 17):e8574–e8574, Dec. 2012. ISSN 1756-

1833. doi: 10.1136/bmj.e8574. URL https://www.bmj.com/lookup/doi/10.1136/bmj.e8574.

Keith E. Dilbeck. Factor Analysis: Varimax Rotation. In *The SAGE Encyclopedia of Communication Research Methods*, volume 4, pages 532–533. SAGE Publications, Inc, 2455 Teller Road, Thousand Oaks California 91320, 2017. ISBN 978-1-4833-8143-5 978-1-4833-8141-1. doi: 10.4135/9781483381411. URL https://methods.sagepub.com/reference/the-sage-encyclopedia-of-communication-research-methods.

I. S. Kim, A. Rauh, E. Wang, and K. Imai. *PanelMatch: Matching Methods for Causal Inference with Time-Series Cross-Sectional Data*. 2022. URL https://CRAN.R-project.org/package=PanelMatch.

A. E. Laureano-Rosario, J. E. Garcia-Rejon, S. Gomez-Carro, J. A. Farfan-Ale, and F. E. Muller-Karger. Modelling dengue fever risk in the State of Yucatan, Mexico using regional-scale satellite-derived sea surface temperature. *Acta Tropica*, 172:50–57, Aug. 2017. ISSN 0001706X. doi: 10.1016/j.actatropica.2017.04.017. URL https://linkinghub.elsevier.com/retrieve/pii/S0001706X1730089X.

C. Li, Z. Zhao, Y. Yan, Q. Liu, Q. Zhao, and W. Ma. Short-term effects of tropical cyclones on the incidence of dengue: a time-series study in Guangzhou, China. *Parasites & Vectors*, 15(1):358, Oct. 2022. ISSN 1756-3305. doi: 10.1186/s13071-022-05486-2. URL https://parasitesandvectors.biomedcentral.com/articles/10.1186/s13071-022-05486-2.

V. S. Limaye, W. Max, J. Constible, and K. Knowlton. Estimating The Costs Of Inaction And The Economic Benefits Of Addressing The Health Harms Of Climate Change. *Health Affairs*, 39(12):2098–2104, Dec. 2020. ISSN 0278-2715. doi: 10.1377/hlthaff.2020.01109. URL https://www.healthaffairs.org/doi/10.1377/hlthaff.2020.01109. Publisher: Health Affairs.

L. Liu, Z. Liu, Y. Wang, and Y. Xu. *fect: Fixed Effects Counterfactuals*. 2022. URL https://CRAN.R-project.org/package=fect.

R. Lowe, A. Gasparrini, C. J. Van Meerbeeck, C. A. Lippi, R. Mahon, A. R. Trotman, L. Rollock, A. Q. J. Hinds, S. J. Ryan, and A. M. Stewart-Ibarra. Nonlinear and delayed impacts of climate on dengue risk in Barbados: A modelling study. *PLOS Medicine*, 15(7):e1002613, July 2018. ISSN 1549-1676. doi: 10.1371/journal.pmed.1002613. URL https://dx.plos.org/10.1371/journal.pmed.1002613.

R. Lowe, S. A. Lee, K. M. O'Reilly, O. J. Brady, L. Bastos, G. Carrasco-Escobar, R. De Castro Catão, F. J. Colón-González, C. Barcellos, M. S. Carvalho, M. Blangiardo, H. Rue, and A. Gasparrini. Combined effects of hydrometeorological hazards and urbanisation on dengue risk in Brazil: a

spatiotemporal modelling study. *The Lancet Planetary Health*, 5(4):e209–e219, Apr. 2021. ISSN 25425196. doi: 10.1016/S2542-5196(20)30292-8. URL https://linkinghub.elsevier.com/retrieve/pii/S2542519620302928.

P. Mahalanobis. On the generalized distance in statistics. *Proc. of the Nation. Acad. Sci.,(India)*, 2:49–5, 1936. URL https://doi.org/10.1007/s13171-019-00164-5.

MapAction. Peru: Flooding, 2023. URL https://maps.mapaction.org/event/2023-per-001.

M. McPherson, A. García-García, F. J. Cuesta-Valero, H. Beltrami, P. Hansen-Ketchum, D. MacDougall, and N. H. Ogden. Expansion of the Lyme Disease Vector *Ixodes Scapularis* in Canada Inferred from CMIP5 Climate Projections. *Environmental Health Perspectives*, 125(5):057008, May 2017. ISSN 0091-6765, 1552-9924. doi: 10.1289/EHP57. URL https://ehp.niehs.nih.gov/doi/10.1289/EHP57.

J. P. Messina, O. J. Brady, N. Golding, M. U. G. Kraemer, G. R. W. Wint, S. E. Ray, D. M. Pigott, F. M. Shearer, K. Johnson, L. Earl, L. B. Marczak, S. Shirude, N. Davis Weaver, M. Gilbert, R. Velayudhan, P. Jones, T. Jaenisch, T. W. Scott, R. C. Reiner, and S. I. Hay. The current and future global distribution and population at risk of dengue. *Nature Microbiology*, 4 (9):1508–1515, Sept. 2019. ISSN 2058-5276. doi: 10.1038/s41564-019-0476-8. URL https://www.nature.com/articles/s41564-019-0476-8. Number: 9 Publisher: Nature Publishing Group.

D. T. Minh An and J. Rocklöv. Epidemiology of dengue fever in Hanoi from 2002 to 2010 and its meteorological determinants. *Global Health Action*, 7(1): 23074, Dec. 2014. ISSN 1654-9716, 1654-9880. doi: 10.3402/gha.v7.23074. URL https://www.tandfonline.com/doi/full/10.3402/gha.v7.23074.

C. Mora, T. McKenzie, I. M. Gaw, J. M. Dean, H. Von Hammerstein, T. A. Knudson, R. O. Setter, C. Z. Smith, K. M. Webster, J. A. Patz, and E. C. Franklin. Over half of known human pathogenic diseases can be aggravated by climate change. *Nature Climate Change*, 12(9):869–875, Sept. 2022. ISSN 1758-678X, 1758-6798. doi: 10.1038/s41558-022-01426-1. URL https://www.nature.com/articles/s41558-022-01426-1.

E. A. Mordecai, J. M. Cohen, M. V. Evans, P. Gudapati, L. R. Johnson, C. A. Lippi, K. Miazgowicz, C. C. Murdock, J. R. Rohr, S. J. Ryan, V. Savage, M. S. Shocket, A. Stewart Ibarra, M. B. Thomas, and D. P. Weikel. Detecting the impact of temperature on transmission of Zika, dengue, and chikungunya using mechanistic models. *PLOS Neglected Tropical Diseases*, 11(4):e0005568, Apr. 2017. ISSN 1935-2735. doi: 10.1371/journal.pntd.0005568. URL https://dx.plos.org/10.1371/journal.pntd.0005568.

E. A. Mordecai, J. M. Caldwell, M. K. Grossman, C. A. Lippi, L. R. Johnson, M. Neira, J. R. Rohr, S. J. Ryan, V. Savage, M. S. Shocket, R. Sippy, A. M.

Stewart Ibarra, M. B. Thomas, and O. Villena. Thermal biology of mosquito-borne disease. *Ecology Letters*, 22(10):1690–1708, Oct. 2019. ISSN 1461-023X, 1461-0248. doi: 10.1111/ele.13335. URL https://onlinelibrary.wiley.com/doi/10.1111/ele.13335.

K. Mulligan, J. Dixon, C.-L. Joanna Sinn, and S. J. Elliott. Is dengue a disease of poverty? A systematic review. *Pathogens and Global Health*, 109(1):10–18, Feb. 2015. ISSN 2047-7724, 2047-7732. doi: 10.1179/2047773214Y.0000000168. URL http://www.tandfonline.com/doi/full/10.1179/2047773214Y.0000000168.

C. V. Munayco, B. Y. Valderrama Rosales, S. Y. Mateo Lizarbe, C. R. Yon Fabian, R. Peña Sánchez, C. H. Vásquez Sánchez, M. P. García, C. Padilla-Rojas, V. Suárez, L. Sánchez-González, F. K. Jones, L. Kohatsu, L. E. Adams, J. Morgan, and G. Paz-Bailey. *Notes from the Field:* Dengue Outbreak — Peru, 2023. *MMWR. Morbidity and Mortality Weekly Report*, 73(4):86–88, Feb. 2024. ISSN 0149-2195, 1545-861X. doi: 10.15585/mmwr.mm7304a4. URL http://www.cdc.gov/mmwr/volumes/73/wr/mm7304a4.htm?s_cid=mm7304a4_w.

H. Murakami, G. A. Vecchi, T. L. Delworth, A. T. Wittenberg, S. Underwood, R. Gudgel, X. Yang, L. Jia, F. Zeng, K. Paffendorf, and W. Zhang. Dominant Role of Subtropical Pacific Warming in Extreme Eastern Pacific Hurricane Seasons: 2015 and the Future. *Journal of Climate*, 30(1):243–264, Jan. 2017. ISSN 0894-8755, 1520-0442. doi: 10.1175/JCLI-D-16-0424.1. URL https://journals.ametsoc.org/doi/10.1175/JCLI-D-16-0424.1.

National Academies of Sciences, Engineering, and Medicine. *Attribution of Extreme Weather Events in the Context of Climate Change*. The National Academies Press, Washington, DC, 2016. ISBN 978-0-309-38094-2. URL https://doi.org/10.17226/21852.

C. Nosrat, J. Altamirano, A. Anyamba, J. M. Caldwell, R. Damoah, F. Mutuku, B. Ndenga, and A. D. LaBeaud. Impact of recent climate extremes on mosquito-borne disease transmission in Kenya. *PLOS Neglected Tropical Diseases*, 15(3):e0009182, Mar. 2021. ISSN 1935-2735. doi: 10.1371/journal.pntd.0009182. URL https://dx.plos.org/10.1371/journal.pntd.0009182.

N. Nova, E. R. Deyle, M. S. Shocket, A. J. MacDonald, M. L. Childs, M. Rypdal, G. Sugihara, and E. A. Mordecai. Susceptible host availability modulates climate effects on dengue dynamics. *Ecology Letters*, 24(3):415–425, Mar. 2021. ISSN 1461-023X, 1461-0248. doi: 10.1111/ele.13652. URL https://onlinelibrary.wiley.com/doi/10.1111/ele.13652.

S. Nyathi, H. C. Karpel, K. L. Sainani, Y. Maldonado, P. J. Hotez, E. Bendavid, and N. C. Lo. The 2016 California policy to eliminate nonmedical vaccine exemptions and changes in vaccine coverage: An empirical policy analysis. *PLOS Medicine*, 16(12):e1002994, Dec. 2019. ISSN 1549-1676.

doi: 10.1371/journal.pmed.1002994. URL https://dx.plos.org/10.1371/journal.pmed.1002994.

N. H. Ogden. Climate change and vector-borne diseases of public health significance. *FEMS Microbiology Letters*, 364(19):fnx186, Oct. 2017. ISSN 0378-1097. doi: 10.1093/femsle/fnx186. URL https://doi.org/10.1093/femsle/fnx186.

N. H. Ogden, M. Radojevic´, X. Wu, V. R. Duvvuri, P. A. Leighton, and J. Wu. Estimated Effects of Projected Climate Change on the Basic Reproductive Number of the Lyme Disease Vector *Ixodes scapularis*. *Environmental Health Perspectives*, 122(6):631–638, June 2014. ISSN 0091-6765, 1552-9924. doi: 10.1289/ehp.1307799. URL https://ehp.niehs.nih.gov/doi/10.1289/ehp.1307799.

Pan American Health Organization / World Health Organization. Epidemiological Update: Increase in dengue cases in the Region of the Americas. Technical report, PAHO/WHO, Washington, D.C., June 2024. URL https://www.paho.org/en/documents/epidemiological-update-increase-dengue-cases-region-americas-18-june-2024.

Q. Peng, S.-P. Xie, G. A. Passalacqua, A. Miyamoto, and C. Deser. The 2023 extreme coastal El Niño: Atmospheric and air-sea coupling mechanisms. *Science Advances*, 10(12):eadk8646, Mar. 2024. ISSN 2375-2548. doi: 10.1126/sciadv.adk8646. URL https://www.science.org/doi/10.1126/sciadv.adk8646.

R Core Team. *R: A Language and Environment for Statistical Computing*. R Foundation for Statistical Computing, Vienna, Austria, 2022. URL https://www.R-project.org/.

K. A. Reed and M. F. Wehner. Real-time attribution of the influence of climate change on extreme weather events: a storyline case study of Hurricane Ian rainfall. *Environmental Research: Climate*, 2(4):043001, Dec. 2023. ISSN 2752-5295. doi: 10.1088/2752-5295/acfd4e. URL https://iopscience.iop.org/article/10.1088/2752-5295/acfd4e.

K. A. Reed, M. F. Wehner, and C. M. Zarzycki. Attribution of 2020 hurricane season extreme rainfall to human-induced climate change. *Nature Communications*, 13(1):1905, Apr. 2022. ISSN 2041-1723. doi: 10.1038/s41467-022-29379-1. URL https://www.nature.com/articles/s41467-022-29379-1.

P. Reiter, S. Lathrop, M. Bunning, B. Biggerstaff, D. Singer, T. Tiwari, L. Baber, M. Amador, J. Thirion, J. Hayes, C. Seca, J. Mendez, B. Ramirez, J. Robinson, J. Rawlings, V. Vorndam, S. Waterman, D. Gubler, G. Clark, and E. Hayes. Texas Lifestyle Limits Transmission of Dengue Virus. *Emerging Infectious Diseases*, 9(1):86–89, Jan. 2003. ISSN 1080-6040, 1080-6059. doi: 10.3201/eid0901.020220. URL http://wwwnc.cdc.gov/eid/article/9/1/02-0220_article.htm.

W. Revelle. psych: Procedures for Psychological, Psychometric, and Personality Research, May 2007. URL https://CRAN.R-project.org/package=psych. Institution: Comprehensive R Archive Network Pages: 2.4.6.26.

S. J. Ryan, C. J. Carlson, E. A. Mordecai, and L. R. Johnson. Global expansion and redistribution of Aedes-borne virus transmission risk with climate change. *PLOS Neglected Tropical Diseases*, 13(3):e0007213, Mar. 2019. ISSN 1935-2735. doi: 10.1371/journal.pntd.0007213. URL https://dx.plos.org/10.1371/journal.pntd.0007213.

L. Schwarz, R. Aguilera, L. C. Aguilar-Dodier, J. E. Castillo Quiñones, M. E. A. García, and T. Benmarhnia. Wildfire smoke knows no borders: Differential vulnerability to smoke effects on cardio-respiratory health in the San Diego-Tijuana region. *PLOS Global Public Health*, 3(6):e0001886, June 2023. ISSN 2767-3375. doi: 10.1371/journal.pgph.0001886. URL https://dx.plos.org/10.1371/journal.pgph.0001886.

N. Scovronick, V. N. Vasquez, F. Errickson, F. Dennig, A. Gasparrini, S. Hajat, D. Spears, and M. B. Budolfson. Human Health and the Social Cost of Carbon: A Primer and Call to Action. *Epidemiology*, 30(5):642–647, Sept. 2019. ISSN 1044-3983. doi: 10.1097/EDE.0000000000001057. URL https://journals.lww.com/10.1097/EDE.0000000000001057.

SENAMHI. Ciclón Yaku se presenta frente al mar peruano, Mar. 2023. URL https://www.gob.pe/institucion/senamhi/noticias/721545-ciclon-yaku-se-presenta-frente-al-mar-peruano.

S. I. Seneviratne, X. Zhang, M. Adnan, W. Badi, C. Dereczynski, A. Di Luca, S. Ghosh, I. Iskandar, J. Kossin, S. Lewis, F. Otto, I. Pinto, M. Satoh, S. M. Vicente-Serrano, M. Wehner, and B. Zhou. Chapter 11: Weather and Climate Extreme Events in a Changing Climate. In V. Masson-Delmotte, P. Zhai, A. Pirani, S. L. Connors, C. Péan, S. Berger, N. Caud, Y. Chen, L. Goldfarb, M. I. Gomis, M. Huang, K. Leitzell, E. Lonnoy, J. B. R. Matthews, T. K. Maycock, T. Waterfield, O. Yelekçi, R. Yu, and B. Zhou, editors, *Climate Change 2021: The Physical Science Basis. Contribution of Working Group I to the Sixth Assessment Report of the Intergovernmental Panel on Climate Change*, pages 1513–1766. Cambridge University Press, Cambridge, United Kingdom and New York, NY, USA, 2021. doi: 10.1017/9781009157896.013.

P. Sheridan, S. McElroy, J. Casey, and T. Benmarhnia. Using the Generalized Synthetic Control Method to Estimate the Impact of Extreme Weather Events on Population Health. *Epidemiology*, 33(6):788–796, Nov. 2022. ISSN 1044-3983. doi: 10.1097/EDE.0000000000001539. URL https://journals.lww.com/10.1097/EDE.0000000000001539.

K. Shioda, J. Cai, J. L. Warren, and D. M. Weinberger. Incorporating Information on Control Diseases Across Space and Time to Improve Estimation of the Population-level Impact of Vaccines. *Epidemiology*, 32(3):360–367,

May 2021. ISSN 1044-3983. doi: 10.1097/EDE.0000000000001341. URL https://journals.lww.com/10.1097/EDE.0000000000001341.

M. S. Shocket, C. B. Anderson, J. M. Caldwell, M. L. Childs, L. I. Couper, S. Han, M. J. Harris, M. E. Howard, M. P. Kai, A. J. MacDonald, N. Nova, and E. A. Mordecai. Environmental Drivers of Vector-Borne Diseases. In *Population Biology of Vector-Borne Diseases*, pages 85–118. Oxford University Press, 2020. ISBN 978-0-19-188771-0. URL https://oxford.universitypressscholarship.com/view/10.1093/oso/9780198853244.001.0001/oso-9780198853244-chapter-6. Publication Title: Population Biology of Vector-Borne Diseases Section: Population Biology of Vector-Borne Diseases.

N. K. Skaff, Q. Cheng, R. E. S. Clemesha, P. A. Collender, A. Gershunov, J. R. Head, C. M. Hoover, D. P. Lettenmaier, J. R. Rohr, R. E. Snyder, and J. V. Remais. Thermal thresholds heighten sensitivity of West Nile virus transmission to changing temperatures in coastal California. *Proceedings of the Royal Society B: Biological Sciences*, 287(1932):20201065, Aug. 2020. ISSN 0962-8452, 1471-2954. doi: 10.1098/rspb.2020.1065. URL https://royalsocietypublishing.org/doi/10.1098/rspb.2020.1065.

A. M. Stewart Ibarra, S. J. Ryan, E. Beltrán, R. Mejía, M. Silva, and Muñoz. Dengue Vector Dynamics (Aedes aegypti) Influenced by Climate and Social Factors in Ecuador: Implications for Targeted Control. *PLoS ONE*, 8(11): e78263, Nov. 2013. ISSN 1932-6203. doi: 10.1371/journal.pone.0078263. URL https://dx.plos.org/10.1371/journal.pone.0078263.

R. F. Stuart-Smith, F. E. L. Otto, A. I. Saad, G. Lisi, P. Minnerop, K. C. Lauta, K. Van Zwieten, and T. Wetzer. Filling the evidentiary gap in climate litigation. *Nature Climate Change*, 11(8):651–655, Aug. 2021. ISSN 1758-678X, 1758-6798. doi: 10.1038/s41558-021-01086-7. URL https://www.nature.com/articles/s41558-021-01086-7.

The Lancet Infectious Diseases. Can we control dengue? *The Lancet Infectious Diseases*, 23(10):1095, Oct. 2023. ISSN 14733099. doi: 10.1016/S1473-3099(23)00578-9. URL https://linkinghub.elsevier.com/retrieve/pii/S1473309923005789.

J. T. Trok, E. A. Barnes, F. V. Davenport, and N. S. Diffenbaugh. Machine learning–based extreme event attribution. *Science Advances*, 10(34):eadl3242, Aug. 2024. ISSN 2375-2548. doi: 10.1126/sciadv.adl3242. URL https://www.science.org/doi/10.1126/sciadv.adl3242.

L. Udayanga, N. Gunathilaka, M. C. M. Iqbal, and W. Abeyewickreme. Climate change induced vulnerability and adaption for dengue incidence in Colombo and Kandy districts: the detailed investigation in Sri Lanka. *Infectious Diseases of Poverty*, 9(1):102, Dec. 2020. ISSN 2049-9957. doi: 10.1186/s40249-020-00717-z. URL https://idpjournal.biomedcentral.com/articles/10.1186/s40249-020-00717-z.

United Nations Office for the Coordination of Humanitarian Affairs. Peru: Flooding and Landslides Situation Report3. Technical Report 3, Apr. 2023. URL https://www.unocha.org/attachments/7da992f8-7722-452a-8cd5-db5311eaa69b/Peru%20OCHA%20Situation%20Report_No%203%20%28ENG%29.pdf.

G. J. Van Oldenborgh, K. Van Der Wiel, A. Sebastian, R. Singh, J. Arrighi, F. Otto, K. Haustein, S. Li, G. Vecchi, and H. Cullen. Attribution of extreme rainfall from Hurricane Harvey, August 2017. *Environmental Research Letters*, 12(12):124009, Dec. 2017. ISSN 1748-9326. doi: 10.1088/1748-9326/aa9ef2. URL https://iopscience.iop.org/article/10.1088/1748-9326/aa9ef2.

L. Vezzulli, C. Grande, P. C. Reid, P. Hélaouët, M. Edwards, M. G. Höfle, I. Brettar, R. R. Colwell, and C. Pruzzo. Climate influence on *Vibrio* and associated human diseases during the past half-century in the coastal North Atlantic. *Proceedings of the National Academy of Sciences*, 113(34), Aug. 2016. ISSN 0027-8424, 1091-6490. doi: 10.1073/pnas.1609157113. URL https://pnas.org/doi/full/10.1073/pnas.1609157113.

A. M. Vicedo-Cabrera, N. Scovronick, F. Sera, D. Royé, R. Schneider, A. Tobias, C. Astrom, Y. Guo, Y. Honda, D. M. Hondula, R. Abrutzky, S. Tong, M. d. S. Z. S. Coelho, P. H. N. Saldiva, E. Lavigne, P. M. Correa, N. V. Ortega, H. Kan, S. Osorio, J. Kyselý, A. Urban, H. Orru, E. Indermitte, J. J. K. Jaakkola, N. Ryti, M. Pascal, A. Schneider, K. Katsouyanni, E. Samoli, F. Mayvaneh, A. Entezari, P. Goodman, A. Zeka, P. Michelozzi, F. de'Donato, M. Hashizume, B. Alahmad, M. H. Diaz, C. D. L. C. Valencia, A. Overcenco, D. Houthuijs, C. Ameling, S. Rao, F. Di Ruscio, G. Carrasco-Escobar, X. Seposo, S. Silva, J. Madureira, I. H. Holobaca, S. Fratianni, F. Acquaotta, H. Kim, W. Lee, C. Iniguez, B. Forsberg, M. S. Ragettli, Y. L. L. Guo, B. Y. Chen, S. Li, B. Armstrong, A. Aleman, A. Zanobetti, J. Schwartz, T. N. Dang, D. V. Dung, N. Gillett, A. Haines, M. Mengel, V. Huber, and A. Gasparrini. The burden of heat-related mortality attributable to recent human-induced climate change. *Nature Climate Change*, 11(6):492–500, June 2021. ISSN 1758-6798. doi: 10.1038/s41558-021-01058-x. URL https://www.nature.com/articles/s41558-021-01058-x. Number: 6 Publisher: Nature Publishing Group.

M. F. Vincenti-Gonzalez, M.-E. Grillet, Z. I. Velasco-Salas, E. F. Lizarazo, M. A. Amarista, G. M. Sierra, G. Comach, and A. Tami. Spatial Analysis of Dengue Seroprevalence and Modeling of Transmission Risk Factors in a Dengue Hyperendemic City of Venezuela. *PLOS Neglected Tropical Diseases*, 11(1): e0005317, Jan. 2017. ISSN 1935-2735. doi: 10.1371/journal.pntd.0005317. URL https://dx.plos.org/10.1371/journal.pntd.0005317.

World Health ORganization. Dengue- Global situation, Dec. 2023. URL https://www.who.int/emergencies/disease-outbreak-news/item/2023-DON498.

Y. Xu. Generalized Synthetic Control Method: Causal Inference with Interactive Fixed Effects Models. *Political Analysis*, 25(1):57–76, Jan. 2017. ISSN 1047-1987, 1476-4989. doi: 10.1017/pan.2016.2. URL https://www.cambridge.org/core/product/identifier/S1047198716000024/type/journal_article.

Y. Zhang, J. Riera, K. Ostrow, S. Siddiqui, H. de Silva, S. Sarkar, L. Fernando, and L. Gardner. Modeling the relative role of human mobility, land-use and climate factors on dengue outbreak emergence in Sri Lanka. *BMC Infectious Diseases*, 20(1):649, Dec. 2020. ISSN 1471-2334. doi: 10.1186/s12879-020-05369-w. URL https://bmcinfectdis.biomedcentral.com/articles/10.1186/s12879-020-05369-w.

6 Supplemental Materials

6.1 Main methods and results

6.1.1 Debiasing temperature data

We compared remotely sensed hourly temperature from ERA5 to monthly average temperatures between 1970 and 2000 reported by the high resolution climatology WorldClim (Fick and Hijmans 2017) following Childs et al. (2024), using the equation:

$$\widehat{ERA5_{ihmy}} = ERA5_{ihmy} - \overline{ERA5_{im}} + \overline{WorldClim_{im}}$$

$\widehat{ERA5_{ihmy}}$ is the debiased ERA5 hourly temperature in a given district (where subscripts i, h, m, and y designate the district, hour, month, and year, respectively), $ERA5_{ihmy}$ is the raw ERA5 hourly temperature in the corresponding district, $\overline{ERA5_{im}}$ and $\overline{WorldClim_{im}}$ are the mean monthly temperatures for a given district from 1970 - 2000 from ERA5 and WorldClim, respectively.

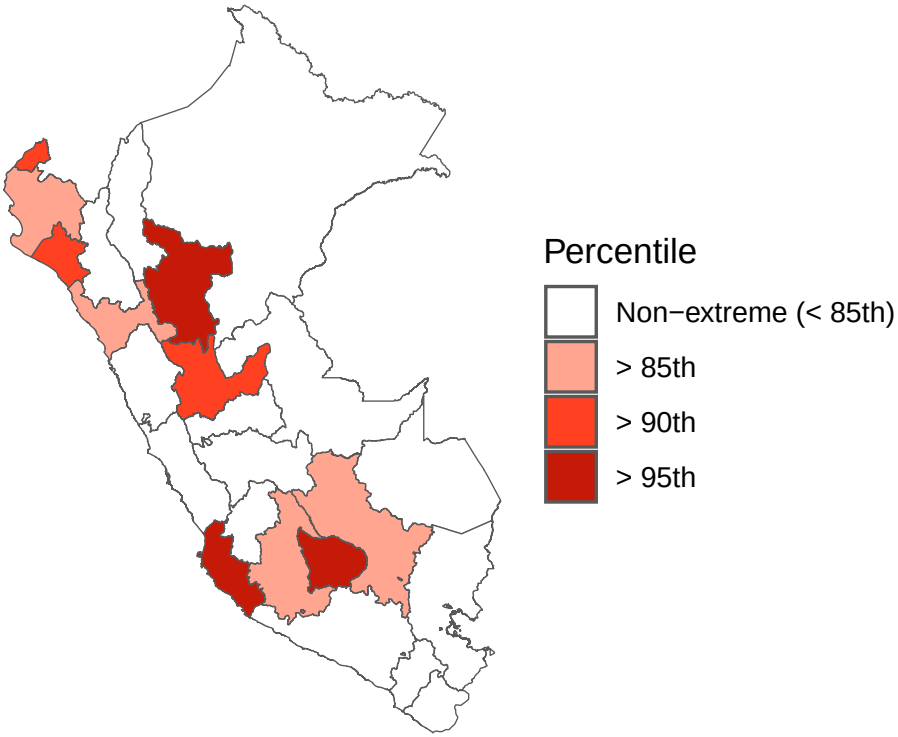

Figure 6: Cyclone-affected districts exceeded the 85th percentile for precipitation during Cyclone Yaku. Precipitation was defined as the average population-weighted total precipitation for each district in the month of March. Precipitation in 2023 (i.e., during Cyclone Yaku) was compared to observations from 1973 - 2022. White indicates regions where precipitation did not exceed the 85th percentile during Cyclone Yaku (i.e., non-extreme), whereas shades of red correspond to precipitation above the 85th percentile, where darker shades of red indicate more extreme precipitatoin.

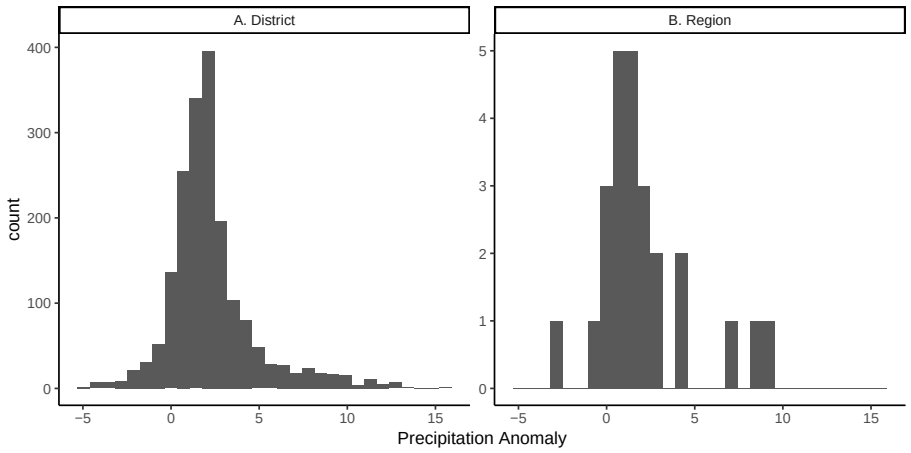

Figure 7: The distribution of precipitation anomalies (mm/day) during Cyclone Yaku at the (A) district and (B) region levels.

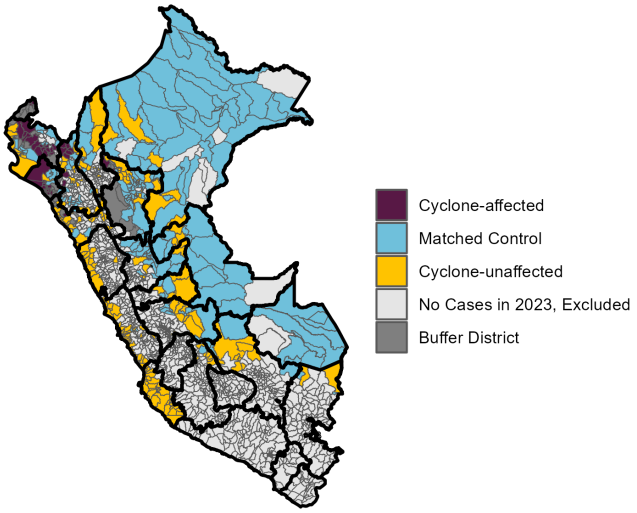

Figure 8: A map of districts in Peru displaying the cyclone-affected (purple) and matched control (blue) districts. Eligible cyclone-unaffected units that were not included in the matched control are shown in yellow. Those excluded from the control set because they did not report cases in 2023 are indicated in light grey while those excluded from the control set because they experienced precipitation anomalies above 7.0 mm/day but below 8.5 mm/day (i.e. buffer districts) are indicated in dark grey. Regional boundaries are indicated with thick black lines.

Region	Province	District
CAJAMARCA	CHOTA	LLAMA

CAJAMARCA	CUTERVO	QUEROCOTILLO
CAJAMARCA	JAEN	SAN JOSE DEL ALTO
CAJAMARCA	SAN IGNACIO	SAN IGNACIO
CAJAMARCA	SAN IGNACIO	CHIRINOS
CAJAMARCA	SAN IGNACIO	LA COIPA
CAJAMARCA	SAN IGNACIO	NAMBALLE
CAJAMARCA	SAN IGNACIO	TABACONAS
LA LIBERTAD	ASCOPE	ASCOPE
LAMBAYEQUE	CHICLAYO	CHICLAYO
LAMBAYEQUE	CHICLAYO	JOSE LEONARDO ORTIZ
LAMBAYEQUE	CHICLAYO	LA VICTORIA
LAMBAYEQUE	CHICLAYO	MONSEFU
LAMBAYEQUE	CHICLAYO	PICSI
LAMBAYEQUE	CHICLAYO	PIMENTEL
LAMBAYEQUE	CHICLAYO	REQUE
LAMBAYEQUE	CHICLAYO	SANTA ROSA
LAMBAYEQUE	CHICLAYO	SAÑA
LAMBAYEQUE	CHICLAYO	POMALCA
LAMBAYEQUE	CHICLAYO	TUMAN
LAMBAYEQUE	FERREÑAFE	FERREÑAFE
LAMBAYEQUE	FERREÑAFE	MANUEL ANTONIO MESONES MURO
LAMBAYEQUE	FERREÑAFE	PUEBLO NUEVO

Table 1: Cyclone-affected district names (continued on next page). Across each row, the columns indicate the region, province, and district names for each cyclone-affected unit.

Region	Province	District
LAMBAYEQUE	LAMBAYEQUE	LAMBAYEQUE
LAMBAYEQUE	LAMBAYEQUE	ILLIMO
LAMBAYEQUE	LAMBAYEQUE	MOCHUMI
LAMBAYEQUE	LAMBAYEQUE	MORROPE
LAMBAYEQUE	LAMBAYEQUE	OLMOS
LAMBAYEQUE	LAMBAYEQUE	PACORA
LAMBAYEQUE	LAMBAYEQUE	SAN JOSE
LAMBAYEQUE	LAMBAYEQUE	TUCUME
PIURA	PIURA	TAMBO GRANDE
PIURA	HUANCABAMBA	HUANCABAMBA
PIURA	HUANCABAMBA	CANCHAQUE
PIURA	HUANCABAMBA	SAN MIGUEL DE EL FAIQUE
PIURA	MORROPON	CHULUCANAS
PIURA	MORROPON	BUENOS AIRES
PIURA	MORROPON	LA MATANZA
PIURA	MORROPON	MORROPON
PIURA	MORROPON	SALITRAL
PIURA	MORROPON	SAN JUAN DE BIGOTE
PIURA	MORROPON	SANTA CATALINA DE MOSSA

PIURA	MORROPON	YAMANGO
PIURA	SULLANA	SULLANA
PIURA	SULLANA	BELLAVISTA
PIURA	SULLANA	LANCONES
PIURA	SULLANA	MARCAVELICA
PIURA	SULLANA	QUERECOTILLO
PIURA	SULLANA	SALITRAL
SAN MARTIN	RIOJA	ELIAS SOPLIN VARGAS
SAN MARTIN	RIOJA	PARDO MIGUEL
TUMBES	TUMBES	TUMBES
TUMBES	TUMBES	SAN JUAN DE LA VIRGEN
TUMBES	ZARUMILLA	ZARUMILLA
TUMBES	ZARUMILLA	AGUAS VERDES
TUMBES	ZARUMILLA	PAPAYAL

Table 1: Cyclone-affected district names (continued from previous page).

6.1.2 Comparing imbalance between cyclone-affected and control districts before and after matching

Prior to matching, heavier precipitation were associated with relatively hotter temperatures in cyclone-affected districts compared to cyclone-unaffected districts. On average, matching favored cyclone-unaffected districts where moderate precipitation (e.g., precipitation exceeding 3 mm/day) coincided with hotter temperatures (above 23°C). Matching is therefore important biologically given that dengue risk depends on the co-occurence of suitable temperature and precipitation conditions – particularly heavy rainfall and warm temperatures. The cyclone-affected units tended to experience greater fluctuations in temperature compared to the cyclone-unaffected districts, although seasonal fluctuations peaked at similar times in both groups (Figure 11B, Table 2). After matching, cyclone-affected districts generally had colder winters compared to the matched control districts but annual maximum temperatures were more similar (meaning that cyclone-affected and control districts had similar temperatures during Cyclone Yaku). Cyclone-affected districts had less precipitation than the control districts, a tendency that remained (and was slightly worsened) after matching (Figure 11A, Table 2). During the cyclone, precipitation in both the cyclone-affected and matched control districts surged but, by definition, deviation from typical conditions was greatest in the cyclone-affected districts (Figure 11A). Given remaining imbalance, we additionally controlled for climate within the generalized synthetic control models. A sensitivity analysis demonstrated that matching did substantially improve alignment between predicted and observed incidence ($R^2 = 0.26$ without matching and $R^2 = 0.60$ with matching, see Figure 23).

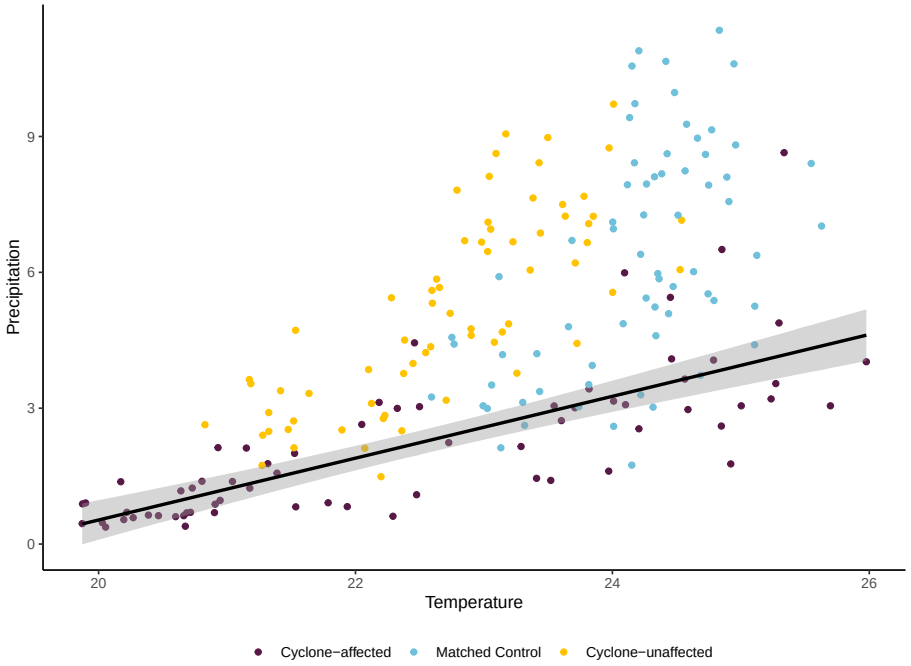

Figure 9: On average, matching selects for districts where the relationship between temperature and precipitation most closely resembles that in the cyclone-affected districts. Each point gives the mean temperature and precipitation at a given pre-cyclone time step across the cyclone-affected districts (purple), matched control pool of cyclone-unaffected districts (blue), and cyclone-unaffected districts prior to matching (purple). The black trendline indicates the linear relationship between temperature and precipitation in the cyclone-affected districts. For the matched control districts, a weighted average of the climate covariates was calculated with weights corresponding to the number of cyclone-affected districts to which a given control district was matched. These values are plotted as a time series in Figure 11.

Group	Mean Temp. (°C)	Sd. Temp. (°C)	Mean Precip. ($\frac{mm}{day}$)	Sd. Precip ($\frac{mm}{day}$)	n
Cyclone-affected	22.6	3.2	2.4	3.7	56
Cyclone-unaffected (Full)	21.4	4.8	4.4	4.3	463
Cyclone-unaffected (Matched)	23.6 (24.3)	4.2 (3.5)	6.5 (6.2)	4.4 (4.4)	194

Table 2: Covariate balance between the cyclone-affected group (first row) and the cyclone-unaffected group before and after matching (second and third rows respectively). The mean and standard deviation of temperature ((°C)) and precipitation (mm/day) are provided. Note, in parentheses, values for the matched control group are weighted by the number of cyclone-affected districts to which each cyclone-unaffected control district was matched.

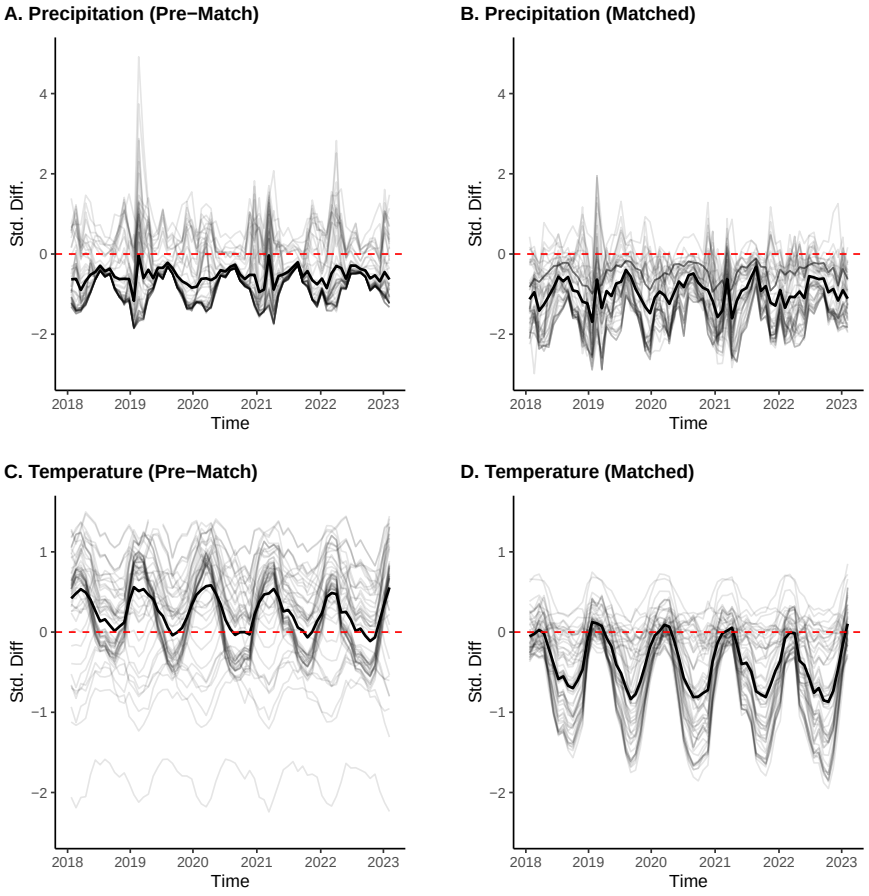

Figure 10: Covariate balance with respect to precipitation (top) and temperature (bottom) before (left) and after (right) matching. Within each panel, each line corresponds to a different cyclone-affected district, comparing its climate covariate values over time to those of either the entire cyclone-unaffected pool prior to matching or the ten cyclone-unaffected control districts to which it was matched. The y-axis corresponds to standardized difference, calculated at each time point as the difference between the value of a given covariate in the cyclone-affected districts compared to the mean value across its corresponding control districts divided by the standard deviation of each climate covariate over the study period. The horizontal dashed line indicates y = 0, or perfect balance. Observations below the line indicate that the value for a given climate covariate in the control units generally exceeds the value for the cyclone-affected units (i.e., hotter or wetter conditions in the control units). The thick black line corresponds to the mean standardized difference across all cyclone-affected districts over time.

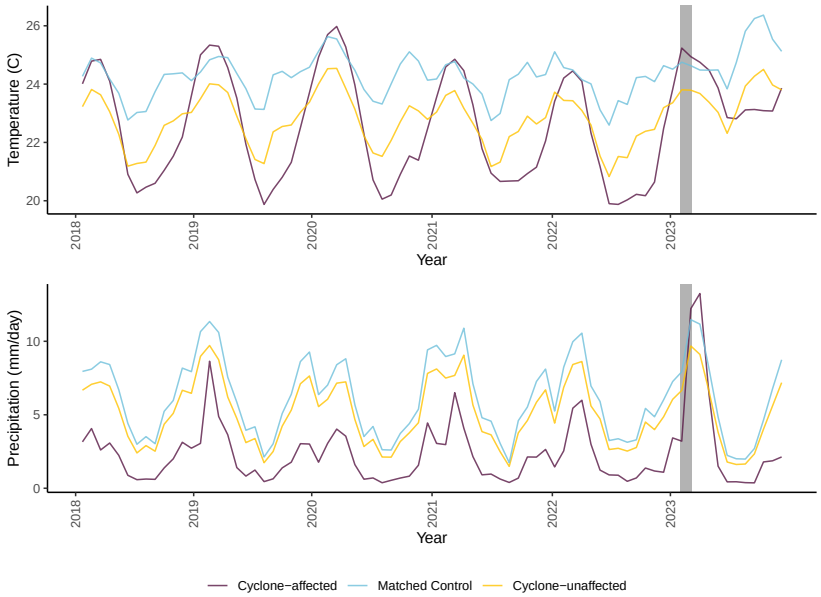

Figure 11: Climate in the cyclone-affected districts (purple) compared to the control pool before (yellow) and after (blue) matching. The top panel shows temperature (°C) and precipitation ($\frac{mm}{day}$) aggregated to 4-week periods from 2018 - 2023, with the x-axis indicating time in years. The grey rectangle indicates the time period when the cyclone occurred in March 2023. Lines display the mean value of precipitation and temperature across the cyclone-affected and cyclone-unaffected districts and a weighted average of the climate covariates across the matched control districts, with weights corresponding to the number of cyclone-affected districts to which a given control district was matched.

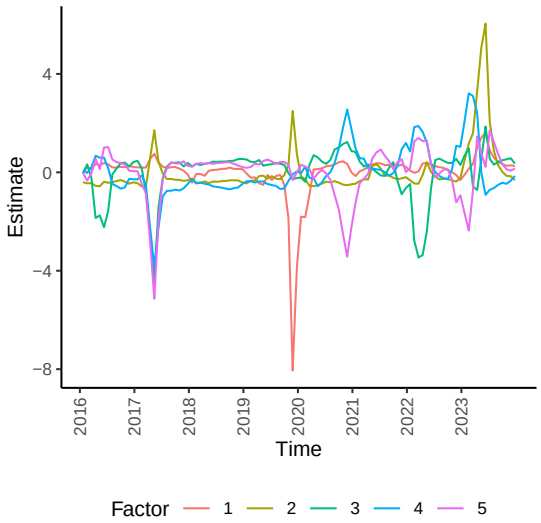

Figure 12: Latent factors estimated from trends in the control districts, accounting for climate covariates. The value of each latent factor (calculated across four-week periods) is plotted over time (x-axis) and each of the five latent factors is indicated in a different color.

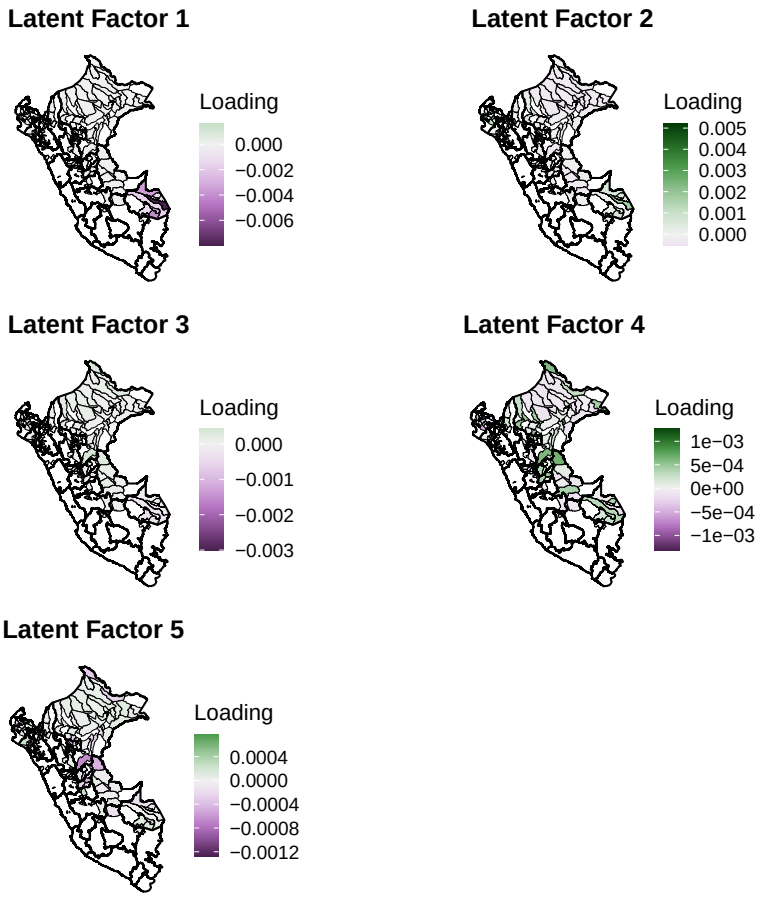

Figure 13: Maps of factor loadings across districts included in the analysis. Panels are maps of Peru with thick lines indicating regions and thin lines indicating districts included in the analysis. Each panel displays the factor loadings for a different latent factor, numbered according to Figure 12, Darker shades of green indicate greater positive values whereas darker shades of purple indicate greater negative values.

Covariate	Coefficient	p-value
Temperature (°C)	$6.60 * 10^{-5}$ $(3.64 * 10^{-5} - 9.55 * 10^{-5})$	0.000
Precipitation (mm/day)	$2.38 * 10^{-5}$ $(8.13 * 10^{-6} - 3.95 * 10^{-5})$	0.003

Table 3: Coefficients (β) estimated for mean temperature and precipitation. We additionally provide bootstrapped 95% confidence intervals and p-values for estimates.

Dates	Percent Attributable Cases	Number Attributable Cases	Obs. Cases	p-value
Pre-cyclone				
Dec 31 - Jan 27	-35 (-374, 75)	-113 (-1224 - 246)	327	0.789
Jan 28 - Feb 24	-24 (-178, 12)	-156 (-1135 - 76)	638	0.910
Feb 25 - Mar 24	-17 (-105, 60)	-268 (-1694 - 969)	1613	0.717
Post-cyclone				
Mar 25 - Apr 21	40 (-33, 77)	2207 (-1789 - 4221)	5493	0.108
Apr 22 - May 19	66 (15, 84)	10303 (2331 - 13110)	15623	0.009
May 20 - Jun 16	67 (27, 88)	12518 (5081 - 16457)	18659	0.002
Jun 17 - Jul 14	64 (28, 90)	6089 (2713 - 8607)	9526	0.002
Jul 15 - Aug 11	65 (13, 92)	3714 (768 - 5247)	5720	0.013
Aug 12 - Sep 08	73 (17, 94)	3149 (753 - 4073)	4317	0.012
Sep 09 - Oct 06	77 (37, 97)	1761 (836 - 2210)	2283	0.003
Oct 07 - Nov 03	60 (-4, 90)	675 (-49 - 1009)	1118	0.037
Nov 04 - Dec 01	47 (-16, 98)	448 (-152 - 930)	947	0.056
Dec 02 - Dec 29	24 (-89, 83)	125 (-456 - 426)	513	0.325

Table 4: Estimated effects of the cyclone on dengue over time across cyclone-affected districts. In order, the columns indicate: the start and end date of the time period (in 2023) across which the cyclone effects were estimated (note that the first time period begins on December 31, 2022) with three pre-cyclone periods included for comparison; the percent of total cases in the cyclone-affected districts attributable to the cyclone with the 95% confidence interval in parentheses; the estimated number of additional cases of dengue across cyclone-affected districts caused by the cylone with the 95% confidence interval in parentheses (negative values indicate cyclone-attributable decreases in cases); the total observed cases across the cyclone-affected districts during the corresponding period; and the p-value of the estimated cyclone effect.

Name	Description	Source
Distance to roads (meters)	50 m resolution raster. Continuous variable. If less than 500 m from the nearest road, 1. If greater than 3000, 0.	MTC. 2020.
Distance to bodies of water and rivers (meters)	50 m resolution raster. Continuous variable. If less than 500 m from the nearest road, 1. If greater than 1500, 0.	MTC. 2023.
Non-public water source	Manzana-level. Proportion of residences not connected to the public water network.	INEI. 2017 National Census.
Inconsistent water access	Manzana-level. Proportion of residences without access to water two or more days per week.	INEI. 2017 National Census.
Household overcrowding	Manzana-level. Proportion of residences with overcrowding (i.e., the of people to rooms in a dwelling is greater than or equal to 3).	INEI. 2017 National Census.
Low-quality walls	Manzana-level. Proportion of residences with walls made from low-quality materials (e.g., plywood, corrugated iron, stone with mud).	INEI. 2017 National Census.
Low-quality floors	Manzana-level. Proportion of residences with floors made from low-quality materials (e.g., dirt).	INEI. 2017 National Census.
Low-quality roofs	Manzana-level. Proportion of residences with roofs made from low-quality materials (e.g., plywood, straw, palm leaf).	INEI. 2017 National Census.
Low-quality residences	Manzana-level. Proportion of residences that were low-quality (e.g., hut or cabin, improvised residence, premises not intended for human residents).	INEI. 2017 National Census.
Susceptibility to flooding	200 m resolution raster. Categorical variable. Forecast for Jan - March 2024. Greatest in areas with steep slopes and little vegetation cover. Values can be: very low (0), low (1), medium (2), high (3), very (high).	CENEPRED. 2023.

Table 5: Vulnerability indices. Each row corresponds to a different vulnerability index, provided by CDC Peru. The first column gives the names of the indices. The second gives descriptions of the indices, including units, resolution, and information on how they were calculated. The third column gives the abbreviated name of the Peruvian agency that provided data for a given index and the year for which it was defined (for the final row, flood risk in 2024 was calculated based on 2023 data). Agency names are abbreviated as following: MTC (Ministerio de Transportes y Comunicaciones, Minister of Transport and Communications); INEI (Instituto Nacional de Estadistica e Informatica, National Institute of Statistcs and Information); CENEPRED (Centro Nacional de Estimación Prevención y Reducción del Riesgo de Desastres, The National Center for Estimation, Prevention and Reduction of Disaster Risk).

Rotated Component	Coefficient	p-value
Low-quality roofs, low-quality walls (RC_1)	5.56 (0.69 - 12.94)	0.12
Low-quality floors, precipitation (RC_2)	-2.53 (-6.57 - 1.45)	0.91
Flood susceptibility, temperature (RC_3)	9.30 (5.92 - 12.95)	0.00
Non-public water source (RC_4)	-0.68 (-6.83 - 4.02)	0.68
Y-intercept (α_3)	13.27 (8.84 - 17.33)	0.00

Table 6: Values estimated for coefficients of the rotated components (derived from vulnerablity indices and climate) and y-intercept. The factors most strongly associated with each rotated components are listed in the first column. We additionally provide bootstrapped 95% confidence intervals and p-values for estimates.

Figure 14: Map of the region of Northwestern Peru used in the climate attribution analysis. A map of Peru is displayed with national borders indicated with thick lines and regional borders indicated with thin lines. The red box indicates the region of northwestern Peru used in the attribution analysis.

6.2 Sensitivity analyses

6.2.1 Sensitivity to exclusion of climate covariates in model

We repeated the main analysis for districts in Peru without including climate covariates in the generalized synthetic control model. Cases were significantly increased by Cyclone Yaku from April 22nd - November 3rd, as was the case for the main model. Overall, we estimate 41,643 (95% confidence interval: 20,398 – 52,228) dengue cases were attributable to Cyclone Yaku, or 73% (95% confidence interval: 36% - 91%) of all cases reported across the cyclone-affected districts during this time period (Figure 15, Figure 17B). Unlike the main model, this model does not generally predict continued fluctuations in case counts during periods of low incidence (Figure 15). The R^2 of this model was equivalent to that of the main model (Figure 17A).

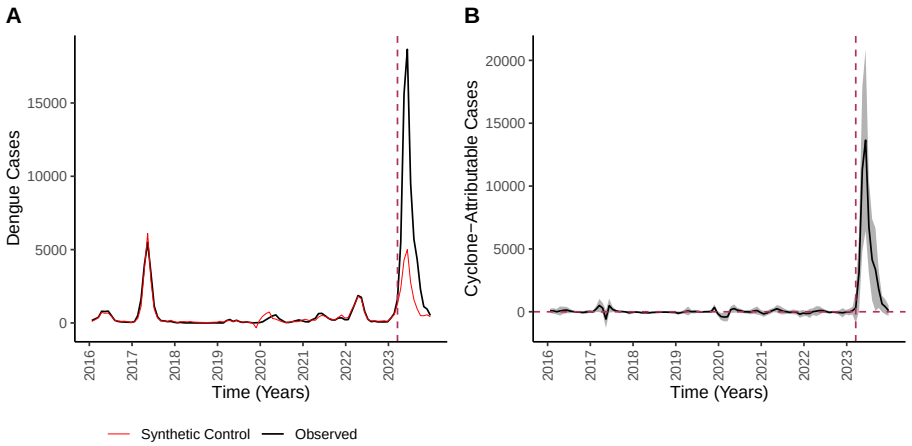

Figure 15: Results of generalized synthetic control analysis without accounting for climate covariates. (A) Shows the total observed cases (black) across all cyclone-affected districts over time compared to the total cases in the synthetic control (red). (B) Shows the effect of the cyclone over time, estimated as the difference between observed cases and synthetic control cases, with the grey ribbon corresponding to the 95% confidence interval. The dashed horizontal line indicates no effect and the dashed vertical line indicates when the cyclone occurred.

6.2.2 Sensitivity to exclusion of non-coastal districts from control pool

In this analysis, the control pool was limited to districts within coastal departments (Tumbes, Piura, Lambayeque, Cajamarca, La Libertad, Ancash, Callao, Lima, Ica, Arequipa, Moquegua, and Tacna) (Figure 8). The cyclone-affected pool was reduced to 54 districts because districts in San Martin that were identified as cyclone-affected in the main text were dropped from this analysis. There were 234 cyclone-unaffected districts and 68 matched control districts in this analysis.

The effect of Cyclone Yaku on cases was significant ($p < 0.05$) from May 20th - June 16th and August 12 - October 6th. At many timepoints in the post-cyclone period, the estimated effect of the cyclone on cases was not significant and confidence intervals encompassed negative values. Across the period that cases were elevated because of the cyclone in the main analysis (April 22nd - November 3rd), we estimate 23,639 (95% confidence interval: 911 – 35,745) cyclone-attributable cases constituting 41% (95% confidence interval: 16% - 62%) of all cases. This is likely a underestimate of the effects of Cyclone Yaku because many coastal districts experienced anomalous precipitation during the cyclone, worsening the control. Further, there may have also been considerable importation of cases from the cyclone-affected districts into neighboring coastal districts. This model had a similar R^2 compared to the model fit to districts across all of Peru ($R^2 = 0.59$) and there was a negligible effect of additionally excluding climate covariates on R^2 ($R^2 = 0.60$) (Figure 17A).

Including climate covariates in the coastal model reduced estimates of the cyclone's effects both by controlling for the fact that 2023 was also unusually rainy because of the coastal El Niño and the tendency of the cyclone-affected provinces in the northwest to have greater precipitation than control provinces along the southern coast (Figure 17B). When climate covariates were excluded, we estimated significant effects of the cyclone on cases from May 20th - July 24th and August 12th - October 6th. Between April 22nd and November 3rd, a total of 24,797 (95% confidence interval: 688 - 40,205) cyclone-attributable cases (43% of cases; 95% confidence interval: 1% - 70%) (Figure 17B).

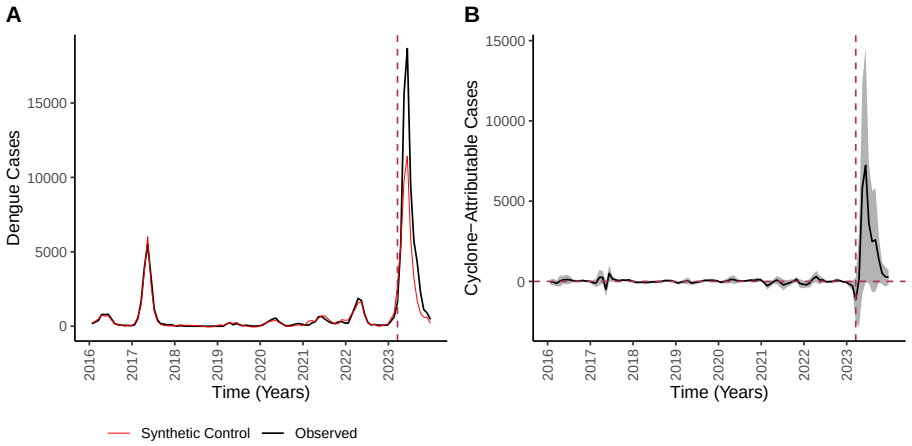

Figure 16: Results of generalized synthetic control analysis across coastal districts. (A) Shows the total observed cases (black) across all cyclone-affected districts over time compared to the total cases in the synthetic control (red). (B) Shows the effect of the cyclone on cases over time, estimated as the difference between observed cases and synthetic control cases, with the grey ribbon corresponding to the 95% confidence interval. The dashed horizontal line indicates no effect and the dashed vertical line indicates when the cyclone occurred.

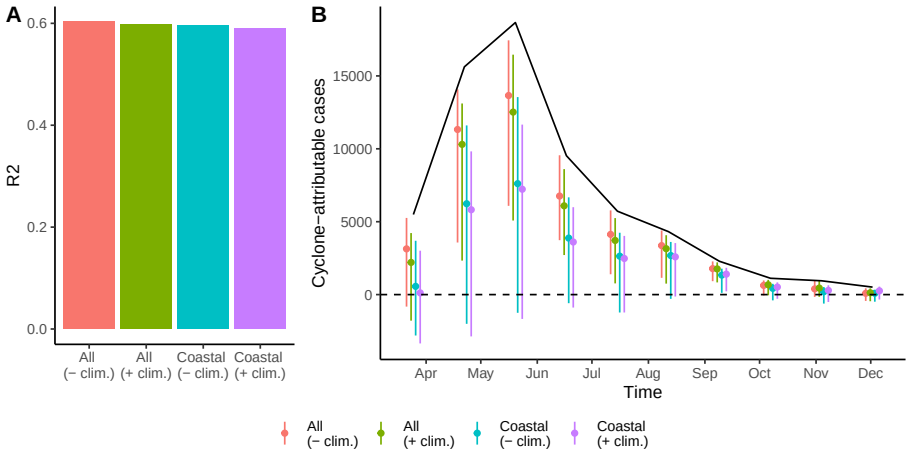

Figure 17: Comparing synthetic control model fit and results depending on whether coastal districts were included in the control pool and whether climate covariates were included in the model. In both panels, we compare models with: all cyclone-unaffected districts in the control pool and no climate covariates (red), all cyclone-unaffected districts in the control pool and climate covariates (green, main model), only coastal cyclone-unaffected districts in the control pool and no climate covariates (blue), and only coastal cyclone-unaffected districts in the control pool and climate covariates (purple). (A) Shows the $R^2$of the generalized synthetic control model depending on model specifications. (B) Shows the estimated effect of the cyclone on cases over time across the cyclone-affected districts (beginning in late March 2023), with the 95% confidence interval. The black line indicates actual cases reported over time in all cyclone-affected districts, including two that are not coastal. The dashed vertical line indicates no effect of the cyclone on cases.

6.2.3 Sensitivity to use of temperature-dependent R_0 as climate covariate in model

Prior work has used laboratory measurements of transmission-relevant traits across a thermal gradient to identify a nonlinear relationship between temperature and relative transmission intensity for dengue (Mordecai et al. 2017). We repeated the main analysis for districts in Peru using temperature-dependent relative R_0 instead of mean temperature as a covariate in the generalized synthetic control model.

Cases were significantly increased by Cyclone Yaku from April 22nd - December 1st Figure 19. We estimate that 36,344 (95% confidence interval: 15,658 - 48,277) or 63% (95% confidence interval: 27% - 84%) of cases were attributable to Cyclone Yaku between April 22nd and November 3rd. These results were similar to those from the main analysis, likely because mean temperature in the study region was generally between 20 and 26$°C$, a range where the relationship between temperature and relative R_0 is expected to be approximately linear.

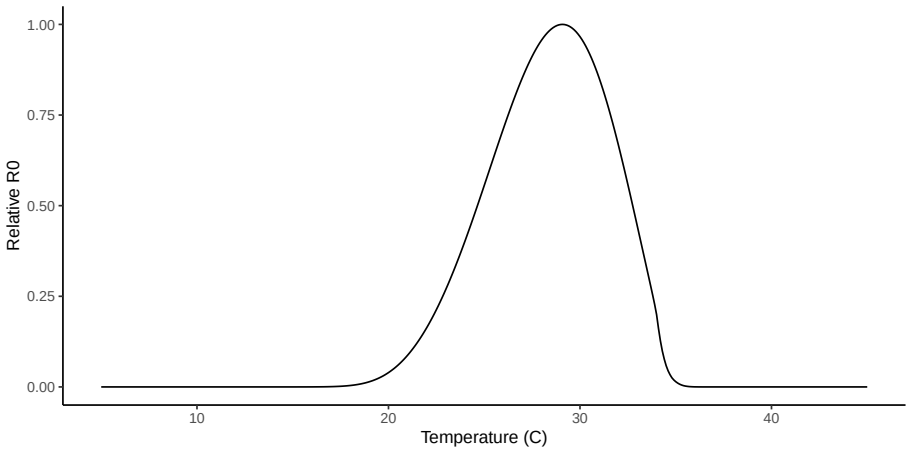

Figure 18: The relationship between temperature (°C) and relative R_0. Relative R_0 is a unitless measure of relative transmission intensity. This relationship was derived by Mordecai et al. (2017) based on laboratory experiments.

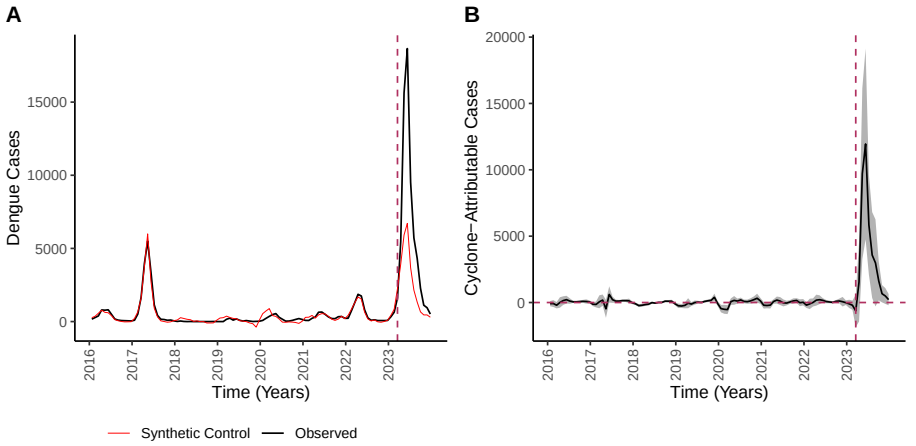

Figure 19: Results of generalized synthetic control analysis using temperature-dependent R_0 instead of mean temperature as a covariate. (A) Shows the total observed cases (black) across all cyclone-affected districts over time compared to the total cases in the synthetic control (red). (B) Shows the effect of the cyclone over time, estimated as the difference between observed cases and synthetic control cases, with the grey ribbon corresponding to the 95% confidence interval. The dashed horizontal line indicates no effect and the dashed vertical line indicates when the cyclone occurred.

6.2.4 Sensitivity to including observations prior to 2016

We conducted the analysis including observations prior to 2016, starting in 2010. We find that cases were significantly increased by Cyclone Yaku across the same period that cases were elevated because of the cyclone according to the main analysis (April 22nd - November 3rd). Across that period, 35,664 (95% confidence interval: 7,175 - 47,047) cases were attributable to the cyclone, or 62% (95% confidence interval: 13% - 82%) of cases, an estimate that is similar to that in the main text. There is a substantial difference between the synthetic control and observed cases during the 2015 outbreak, although this difference is considerably smaller than that observed during the 2023 outbreak. The synthetic control also regularly exceeds observed outbreaks prior to 2015.

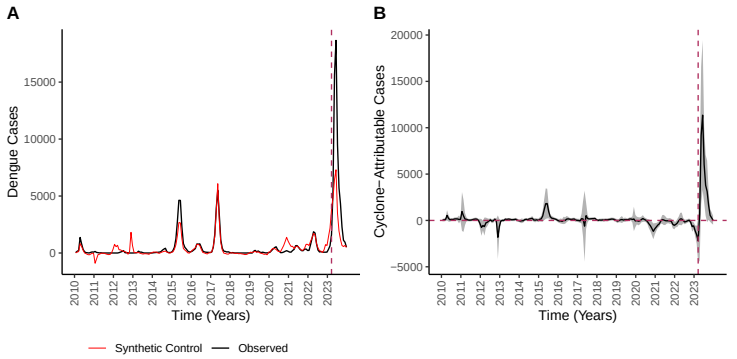

Figure 20: Results of generalized synthetic control analysis including observations prior to 2016. (A) Total observed cases (black) across all cyclone-affected districts over time compared to the total cases in the synthetic control units (red). (B) Effect of the cyclone over time, estimated as the difference between observed cases and synthetic control cases. The dashed horizontal line indicates no effect and the dashed vertical line indicates when the cyclone occurred.

6.2.5 Sensitivity to excluding observations from 2020 - 2021

We conducted the analysis excluding observations from 2020 - 2021 due to the potential for substantial biases in reporting during the beginning of the COVID-19 pandemic. To conduct this analysis, we additionally included observations from 2010 - 2016 so that a sufficient number of years of observations were used to fit the model. We find that cases were significantly increased by Cyclone Yaku between April 22nd and December 1st (Figure 21). Between April 22nd and November 3rd, 44,314 (95% confidence interval: 36,844 - 49,729) cases were attributable to Cyclone Yaku, or 77% (95% confidence interval: 64% - 87%) of all cases.

This estimate is similar to that from the main analysis, suggesting that potential biases in case reporting during the COVID-19 pandemic did not substantially affect our results. Cases were generally low during this time period across the cyclone-affected districts and variation in dengue cases over time connected to the COVID-19 pandemic that were consistent across the study region were accounted for by the latent factors (Figure 2).

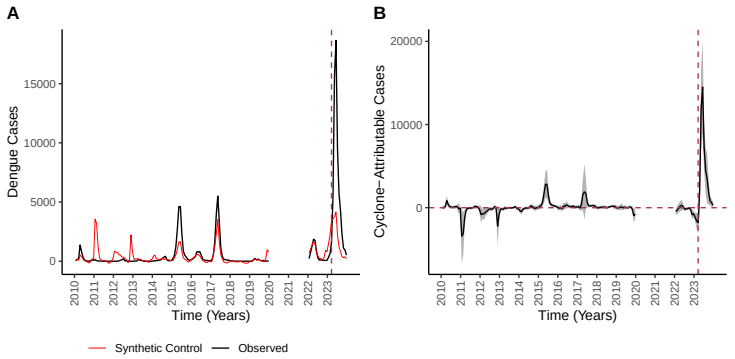

Figure 21: Results of generalized synthetic control analysis excluding observations from 2020 and 2021. (A) Total observed cases (black) across all cyclone-affected districts over time compared to the total cases in the synthetic control units (red). (B) Effect of the cyclone over time, estimated as the difference between observed cases and synthetic control cases. The dashed horizontal line indicates no effect and the dashed vertical line indicates when the cyclone occurred. Years excluded from the analysis are shown as a gap in the plot.

6.2.6 Sensitivity to upper and lower precipitation anomaly thresholds

We repeated the analysis varying the upper precipitation anomaly threshold above which districts were included in the cyclone-affected group and the lower precipitation anomaly threshold below which districts were included in the cyclone-unaffected group. Note that more districts are included in the cyclone-affected group when the upper threshold is lowered, increasing the number of observed cases under consideration. All numbers and percentages of attributable cases reported here were calculated from April 22nd to November 3rd to facilitate comparison with the main model.

When the upper threshold is fixed at 8.5 mm/day and the lower threshold is increased to 8.5 mm/day, the balance with respect to precipitation and temperature increased, while climate covariate balance decreased when the lower threshold was reduced to 5.5 mm/day. In both cases, R^2, our measure of model fit (where greater values indicate better fit), decreases compared to the main model (for lower thresholds of 8.5 mm/day: $R^2 = 0.34$; for lower threshold of 5.5 mm/day: $R^2 = 0.31$). The estimate of the percentage of cases attributable to the cyclone decreases with a lower threshold of 8.5 mm/day to 41% (95% confidence interval: -1% - 81%) and also decreases with a lower threshold of 5.5 mm/day to 41% (95% confidence interval: -7% - 121%). Notably, there is considerably more uncertainty for both of these estimates.

When the upper threshold is increased to 10 mm/day, the percentage of attributable cases is 71% (95% confidence interval: 21% - 107%), 76% (95% confidence interval: 55% - 88%), 15% (95% confidence interval: -38% - 79%), and -11% (95% confidence interval: -50% - 75%) for lower thresholds of 5.5, 7, 8.5, and 10 mm/day, respectively. These estimates are slightly greater than those in

the main analysis, potentially indicating that the cyclone had greater impacts in districts with the greatest precipitation anomalies. R^2 was considerably worse or comparable to that of the main model for a greater upper threshold.

The estimate of the percent of cases attributable to the cyclone with an upper threshold of 7 mm/day and lower threshold of 7 mm/day is similar to that of the main model: 68% (95% confidence interval: 45% - 83%) of total cases. When the lower threshold is reduce to 5.5 mm/day, we estimate that 45% (95% confidence interval: 5% - 120%) of cases were attributable to the cyclone. The large uncertainty on these estimates and fact that the latter exceeds 100% suggests that there is an insufficient number of control districts to construct a robust synthetic control for the larger set of 98 cyclone-affected districts. Indeed, R^2 was reduced for this model ($R^2 = 0.41$).

The general pattern of an increase in the estimated cyclone effect when the lower threshold is reduced suggests that cyclone effects may be observed in districts with precipitation anomalies greater than 5.5 mm/day and that the main analysis therefore underestimates the true number of cyclone attributable cases, for several reasons. First, additional cyclone-affected districts were excluded from our main analysis. Second, the inclusion of these districts in the control pool may bias our estimate of the cyclone effects downward. However, decreasing the lower and upper thresholds reduces the number of control districts while increasing the number of cyclone-affected districts, worsening the balance and model fit.

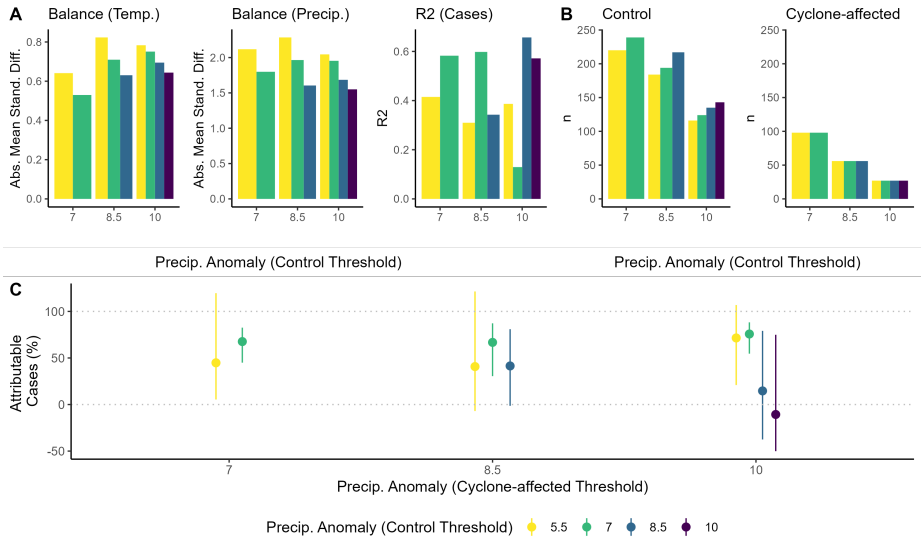

Figure 22: The effects of varying the upper and lower precipitation anomaly threshold. The x-axis of each panel is the upper precipitation anomaly threshold. The colors of the bars correspond to the lower precipitation anomaly threshold (legend at bottom). (A) The balance between the cyclone-affected and matched control units with respect to climate covariates and the prediction error of the resulting generalized synthetic control model depending on upper and lower anomaly thresholds. The first two graphs show balance with respect to temperature (left) and precipitation (middle). Balance is the difference in climate conditions between the cyclone-affected and control units, measured as the average absolute standardized difference across the study period (Figure 10). The final graph (right) shows R^2, a measure of the difference between the observed and predicted (synthetic control) cases in the cyclone-affected districts prior to Cyclone Yaku. (B) The size of the matched control (left) and cyclone-affected (right) groups. (C) The estimated percentage of cases observed across all cyclone-affected districts that were attributable to the cyclone between April 22nd and November 3rd. The bars indicate 95% confidence intervals.

6.2.7 Sensitivity to number of matched units

We repeated the main analysis varying the number of control units to which each cyclone-affected unit was matched. Increasing or decreasing the number of units to match to had little effect on the estimated percentage of cases attributable to the cyclone (Figure 23). Including all cyclone-unaffected units in the control pool for the generalized synthetic control model leads to a lower estimate of attributable cases (48% of all cases from April 22nd to November 3rd), although there is considerable uncertainty in this estimate (95% confidence interval: -4% - 76%) and reduced predictive accuracy compared to the main model ($R^2 = 0.26$).

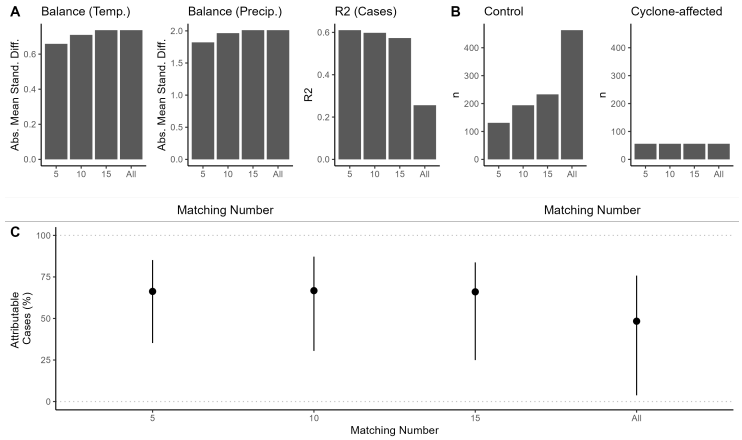

Figure 23: The effects of varying the number of control districts matched to each cyclone-affected district (x-axis). Note that "all" indicates that no matching was performed and all cyclone-unaffected districts were included in the generalized synthetic control analysis. (A) The balance between the cyclone-affected and matched control units with respect to climate covariates and the prediction error of the resulting generalized synthetic control model depending on number of matched units. The first two graphs show balance with respect to temperature (left) and precipitation (middle). Balance is measured as the mean absolute value of the standardized difference across the study period (Figure 10). The final graph (right) shows the R^2, a measure of the difference between the observed and predicted (synthetic control) cases in the cyclone-affected districts prior to Cyclone Yaku. (B) The size of the matched control (left) and cyclone-affected (right) groups. (C) The estimated percentage of cases observed across all cyclone-affected districts that were attributable to the cyclone between April 22nd and November 3rd. The bars indicate 95% confidence intervals.

6.2.8 Sensitivity to number of latent factors

We repeated the main analysis, varying the number of latent factors included in the generalized synthetic control model from zero to five. As described in the main text, the number of latent factors was selected to minimize mean squared prediction error calculated through a cross-validation procedure and five latent factors were therefore included in the main model. The estimated percentage of attributable cases is relatively stable across different numbers of latent factors, ranging from 63% with four latent factors to 82% with three latent factors.

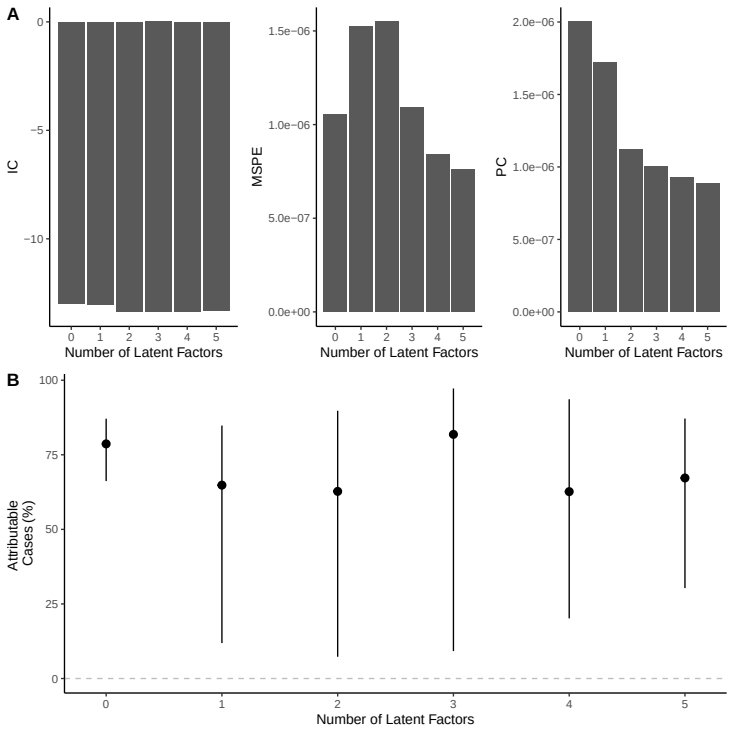

Figure 24: The effects of varying the number of latent factors (x-axis). (A) The model fit depending on the number of latent factors. Graphs show the information criterion (IC), proposed criterion (PC), and root mean squared error (RMSE). (B) The estimated proportion of cases observed across all cyclone-affected districts that were attributable to the cyclone (from April 22nd - November 3rd) depending on the number of latent factors. The bars indicate 95% confidence intervals.

6.2.9 Analysis at the region level

We repeated the analysis at the region level to estimate cyclone effects at a large scale. Because there are only 25 regions (plus a capital district) in Peru, we expanded our dataset by compiling weekly case reports at administrative division 1 across four additional countries in Latin America: Ecuador, Brazil, Mexico, and Colombia. Data were obtained through public, online data portals

except in the case of Ecuador, where data were provided by the Surveillance and Epidemiological Office of the Ministry of Health (Table 7). Countries were selected based on data availability and proximity to the cyclone-affected regions in Peru.

Data were collected from the earliest date availability through the end of 2023 or the latest date in 2023 available. This analysis ends in late July 2023 because case data for Colombia and Ecuador were not yet available beyond that time point. Because significant effects of Cyclone Yaku on cases were detected through December in the main analysis, this represents an incomplete estimate. Piura, Tumbes, and Lambayeque regions in Peru were identified as cyclone-affected units given that their precipitation anomalies during Cyclone Yaku above 7 mm/day were clear outliers compared to other departments in Peru (Figure 7B). Regions across all countries with anomalies below 7 mm/day were eligible to be included in the control pool.

Significant effects of Cyclone Yaku on cases were first detected in the period from February 25 - March 24, during which the cyclone occurred. We estimate that 85,946 (95% confidence interval: 81,342 - 87,143) cases were attributable to Cyclone Yaku out of 88,373 cases, or 97% (95% confidence interval: 92% - 99%) of all cases from April 22nd - July 14th (the period across which data were available and significant cyclone effects were detected). The synthetic control may be a less appropriate predictor of cases at the region level because dengue dynamics and associated covariates may vary considerably across regions and countries, meaning that the generalized synthetic control model may fail to capture latent trends relevant to the cyclone-affected departments based on observations across the control pool.

Country	Start Year	End Month	No. units	No. units with data	Source
Brazil	2014	Dec	27*	27*	online
Colombia	2013	Jul	33*	33*	online
Ecuador	2014	Aug	24	24	MoH
Mexico	2003	Dec	32*	30	online
Peru	2000	Dec	26*	25	online

Table 7: Data sources for administrative division 1. Columns indicate the country name, starting year of data available (with all datasets starting in epiweek one), ending month of data for 2023 available, the number of spatial units in the country, the number of spatial units with data available, and the data source (with hyperlinks to online web portals). * indicates counts that include a capital district.

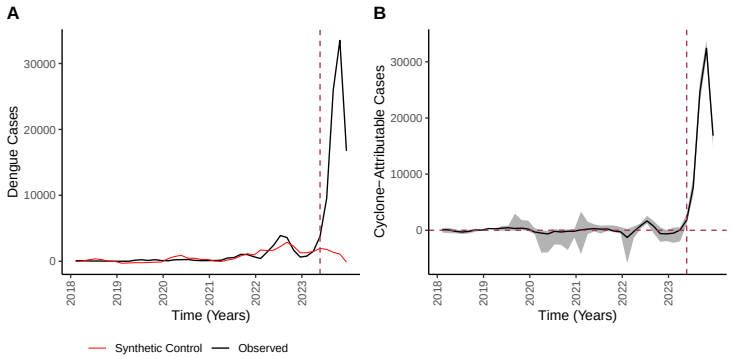

Figure 25: Results of generalized synthetic control analysis at the region level. (A) Shows the total observed cases (black) across all cyclone-affected departments over time compared to the total cases in the synthetic control (red). (B) Shows the effect of the cyclone over time, estimated as the difference between observed cases and synthetic control cases, with the grey ribbon corresponding to the 95% confidence interval. The dashed horizontal line indicates no effect and the dashed vertical line indicates when the cyclone occurred.